Therapeutic antiviral T cells noncytopathically clear persistently infected microglia after conversion into antigen-presenting cells

Jasmin Herz, Kory R. Johnson, and Dorian B. McGavern

National Institute of Neurological Disorders and Stroke, National Institutes of Health, Bethesda, MD 20892

Several viruses can infect the mammalian nervous system and induce neurological dysfunction. Adoptive immunotherapy is an approach that involves administration of antiviral T cells and has shown promise in clinical studies for the treatment of peripheral virus infections in humans such as cytomegalovirus (CMV), Epstein–Barr virus (EBV), and adenovirus, among others. In contrast, clearance of neurotropic infections is particularly challenging because the central nervous system (CNS) is relatively intolerant of immunopathological reactions. Therefore, it is essential to develop and mechanistically understand therapies that noncytopathically eradicate pathogens from the CNS. Here, we used mice persistently infected from birth with lymphocytic choriomeningitis virus (LCMV) to demonstrate that therapeutic antiviral T cells can completely purge the persistently infected brain without causing blood–brain barrier breakdown or tissue damage. Mechanistically, this is accomplished through a tailored release of chemoattractants that recruit antiviral T cells, but few pathogenic innate immune cells such as neutrophils and inflammatory monocytes. Upon arrival, T cells enlisted the support of nearly all brain-resident myeloid cells (microglia) by inducing proliferation and converting them into CD11c$^+$ antigen-presenting cells (APCs). Two-photon imaging experiments revealed that antiviral CD8$^+$ and CD4$^+$ T cells interacted directly with CD11c$^+$ microglia and induced STAT1 signaling but did not initiate programmed cell death. We propose that noncytopathic CNS viral clearance can be achieved by therapeutic antiviral T cells reliant on restricted chemoattractant production and interactions with apoptosis-resistant microglia.

CORRESPONDENCE
Dorian B. McGavern:
mcgavernd@mail.nih.gov

Abbreviations used: aCSF, artificial cerebral spinal fluid; BBB, blood–brain barrier; CNS, central nervous system; LCMV, lymphocytic choriomeningitis virus; NP, nucleoprotein; Q-PCR, quantitative PCR; PFA, paraformaldehyde; RT, room temperature; tg, transgenic; TPLSM, two-photon laser-scanning microscopy; TUNEL, terminal deoxynucleotidyl transferase-mediated UTP nick end-labeling.

The sophistication and irreparable components of the central nervous system (CNS) require strict modulation of potentially damaging inflammatory responses. Despite residing behind a tight barrier system, the CNS is susceptible to infection by many neurotropic viruses (van den Pol, 2006; Tyler, 2009a,b; McGavern and Kang, 2011). Some viruses replicate there acutely, inducing neurological complications, whereas others establish lifelong persistence and chronically disrupt CNS homeostasis. The mechanisms that allow viruses to enter and ultimately inhabit the CNS are varied. Through the process of evolution, many viruses have acquired immunosuppressive strategies that allow them to interfere with innate and adaptive immune mechanisms. For example, a common approach used by neurotropic viruses is to target the type I IFN (IFN-I) pathway (Haller et al., 2006), which is one of the most important antiviral defense systems used by the CNS (Nayak et al., 2013). Another susceptibility factor for viral entry stems from immune-dampening mechanisms like IL-10 and PD-1, which are routinely used by the CNS and other tissues to lessen the intensity of immune responses and preserve tissue integrity (Barber et al., 2006; Brooks et al., 2006; Phares et al., 2012; Zinselmeyer et al., 2013). The downside of immunoregulatory mechanisms is that the CNS can be targeted by viruses as immune pressure wanes. In fact, the magnitude of CNS viral spread can mirror the state of functional immune exhaustion in the periphery (Lauterbach et al., 2007), and many viruses like HIV-1 and John Cunningham (JC) virus exploit weakened immune defenses to gain access to the CNS (McGavern and Kang, 2011; Ousman and Kubes, 2012).

Understanding the immunological mechanisms that give rise to tissue destruction in the

The Rockefeller University Press $30.00
J. Exp. Med. 2015 Vol. 212 No. 8 1153–1169
www.jem.org/cgi/doi/10.1084/jem.20142047

The Journal of Experimental Medicine

virally infected brain is crucial if we intend to therapeutically resolve persistent infections without inducing permanent neurological dysfunction. It is well described that antiviral T cells are equipped with cytopathic effector mechanisms such as perforin and granzymes that are known to cause cell death and tissue pathology (Kägi et al., 1996; Moseman and McGavern, 2013). For example, destruction of virus-infected cells by cytotoxic lymphocytes is a major cause of tissue injury after CNS infection by West Nile virus and human CMV (Ousman and Kubes, 2012). Even the antiviral cytokine IFNγ can play a pathogenic role in the inflamed brain by fostering destruction of CNS architecture (Horwitz et al., 1997; Kreutzfeldt et al., 2013). Another mode of pathogenesis involves the recruitment of innate accessory cells such as monocytes and neutrophils that induce destruction of the blood–brain barrier (BBB) and blood–cerebrospinal fluid barrier during the process of extravasation (Kim et al., 2009; Howe et al., 2012). This pathogenic recruitment of innate immune cells into the virally infected CNS is driven in part by the direct release of chemoattractants by antiviral T cells (Kim et al., 2009). Thus, it is clear that antiviral T cells possess an abundance of mechanisms to damage the CNS upon viral infection.

A primary challenge in the biomedical research community is devising efficacious strategies to purge viral infections. Prevention of infection through vaccination has yielded a myriad of successes (Plotkin, 2009; Koff et al., 2013), but therapeutic elimination of viruses has proven more difficult to accomplish, particularly during states of persistence (Nath and Tyler, 2013). One approach that is gaining considerable momentum is referred to as adoptive immunotherapy or immunocytotherapy (Volkert, 1962, 1963; Oldstone et al., 1986). This approach involves the therapeutic administration of antiviral T cells into a virally infected host. The original description of adoptive immunotherapy involved use of mice persistently infected from birth with lymphocytic choriomeningitis virus (LCMV), often referred to as LCMV carrier mice (Kang and McGavern, 2008). Remarkably, adoptive transfer of memory splenocytes from an LCMV immune mouse into a persistently infected carrier yielded systemic viral clearance (Volkert, 1962, 1963; Oldstone et al., 1986). It was subsequently revealed that this process was dependent on LCMV-specific memory $CD8^+$ and $CD4^+$ T cells (Berger et al., 2000), antiviral cytokines (IFNγ, TNF, and IFN-I; Tishon et al., 1995; Planz et al., 1997; Lauterbach et al., 2006), and interactions with recipient APCs (Jamieson et al., 1987; Lauterbach et al., 2006). This therapy has since been translated into humans with the original study showing that adoptive transfer of CMV-specific $CD8^+$ T cells into patients receiving bone marrow transplants could confer protection against fatal CMV pneumonia (Riddell et al., 1992). A similar strategy was used to successfully treat patients with EBV-induced lymphoproliferative disorders (Heslop et al., 1994; Papadopoulos et al., 1994). Adoptive immunotherapeutic approaches have advanced rapidly over the years and now include methods to generate T cells specific to multiple viruses (Leen et al., 2006; Papadopoulou et al., 2014) or T cells genetically engineered to express chimeric antigen receptors that provide an enhanced targeting potential (Scholler et al., 2012).

Although adoptive immunotherapies offer a means to clear established peripheral infections, it is unclear whether this approach will be comparably successful in eradicating neurotropic viruses given the unique challenges imposed on the immune system by the CNS. Thus, it is important to define the mechanisms underlying pathogenic versus nonpathogenic T cell interactions in the virally infected CNS. The LCMV model system has proven instrumental in this regard (McGavern et al., 2002b; Kang and McGavern, 2008). LCMV is a noncytopathic arenavirus that infects both rodents and humans. Because the virus is noncytopathic, any pathology observed in the LCMV-infected brain is caused by the immune system rather than the virus per se. Intracerebral inoculation of mice with LCMV induces fatal meningitis mediated by $CD8^+$ T cells and myelomonocytic cells (Kim et al., 2009; McGavern and Kang, 2011). In contrast, therapeutic administration of antiviral T cells to LCMV carrier mice results in CNS viral clearance without death of the host (Volkert, 1962, 1963; Oldstone et al., 1986). We therefore set out to determine the factors that allow antiviral T cells to operate in the virally infected brain without inducing overt neurological symptoms or disease. Interestingly, we uncovered that antiviral T cells can purge the persistently infected brain in the complete absence of vascular or tissue pathology. This is accomplished through tailored chemoattractant release that selectively recruits antiviral T cells (in the absence of myelomonocytic cells), which then interact with and convert microglia into apoptosis-resistant APCs.

RESULTS

Therapeutic memory T cells clear the persistently infected brain in the absence of tissue injury

After adoptive immunotherapy, persistently infected neurons in LCMV carrier mice can be purged over a 100-d period (Oldstone et al., 1986; Ahmed et al., 1987). Because antiviral T lymphocytes with a pathogenic potential enter the CNS parenchyma within the first 1–2 wk after transfer (Lauterbach et al., 2006), we initially set out to evaluate the magnitude of CNS injury during the peak T cell infiltration period. This was accomplished by quantifying cytopathology on tissue sections using TUNEL (terminal deoxynucleotidyl transferase-mediated UTP nick end-labeling) staining (Fig. 1, A and B) and by assessing BBB leakage with an Evans blue assay (Fig. 1, C–E). Adult LCMV carrier mice persistently infected from birth received adoptive immunotherapy and were processed on day 9 or 30. As a positive control for BBB breakdown and cytopathology, we analyzed mice with LCMV meningitis on day 6 after infection (McGavern et al., 2002a). As expected, a marked increase in apoptosis was observed on day 6 sagittal brain sections from mice with meningitis relative to naive controls (Fig. 1 A). In contrast, no increase in apoptosis was detected on brain sections from day 9 immunotherapy recipients. To determine whether the absence of cytopathology

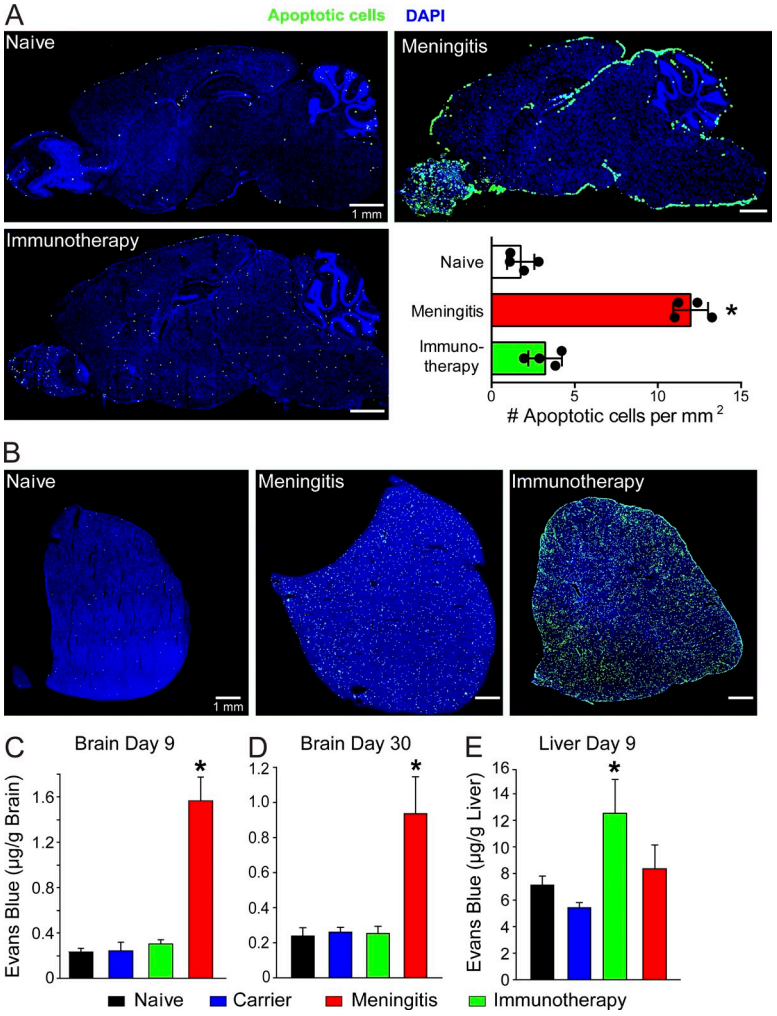

Figure 1. Absence of tissue injury during viral clearance of the persistently infected brain. (A) Cell death was assessed in the brains of mice with fatal meningitis or after adoptive immunotherapy by performing TUNEL staining. 9 d after adoptive immunotherapy, frozen sagittal brain sections from LCMV carrier mice were stained to detect apoptotic cells and cell nuclei (DAPI) and compared with uninfected control tissue, as well as brain sections from symptomatic day 6 mice with LCMV meningitis (positive control for apoptosis). The bar graph depicts the mean ± SD for each group, and each symbol is an individual mouse ($n = 4$ mice per group). (B) TUNEL staining was performed on liver tissue extracted from the same groups of mice as above. Note the increased number of apoptotic cells on the liver section from the day 9 immunotherapy recipient when compared with the naive and day 6 meningitis tissues. (C–E) Vascular leakage was assessed using an Evans Blue assay at day 9 (C and E) and day 30 (D) after immunotherapy in the brain (C and D) and liver (E). Naive and LCMV carrier mice not receiving immunotherapy served as negative control for this experiment. Mice with LCMV meningitis at day 6 after infection served as a positive control for vascular leakage in the brain. Bar graphs show the mean ± SD for each group ($n = 4$ mice per group). All data shown in this figure are representative of three independent experiments. Asterisks denote statistical significance (*, $P < 0.05$).

was unique to the brain, we examined liver tissue from LCMV carrier mice at the same time point and observed a massive increase in apoptosis (Fig. 1 B). These data indicate that the liver develops intense cytopathology after immunotherapy, whereas the brain is spared. This conclusion was corroborated by Evans blue leakage assays, which revealed significant disruption of the BBB in mice with LCMV meningitis, but no leakage in the CNS of immunotherapy recipients at day 9 or 30 (Fig. 1, C and D). However, Evans blue leakage was observed in the liver of immunotherapy recipients at day 9, consistent with the increased apoptosis (Fig. 1 E).

Immunotherapy promotes tailored chemokine expression with minimal myelomonocytic cell infiltration

We recently demonstrated that fatal immunopathology during LCMV meningitis is caused in part by CTL-induced recruitment of pathogenic myelomonocytic cells into the CNS on day 6 after infection (Kim et al., 2009). To provide an explanation for the absence of CNS pathology in immunotherapy recipients, we evaluated the composition of the immune infiltrate at day 9 (Fig. 2 A). A comparable number of CNS-infiltrating CD8 T cells was observed in immunotherapy recipients relative to mice with meningitis. In addition, the number of traceable LCMV TCR transgenic (tg) $CD8^+$ T cells (referred to as P14 cells; Pircher et al., 1989) and CD4 T cells was also slightly elevated in the CNS of immunotherapy recipients despite the minimal pathology (Fig. 2 A). The most striking difference between immunotherapy recipients and mice with meningitis emerged after quantification of innate myelomonocytic cells. These cells heavily infiltrated the brains of mice with fatal meningitis but were not present in the CNS of immunotherapy recipients (Fig. 2 A). This pattern of immune infiltration was specific to the CNS, as a significant increase in myelomonocytic cells was observed in the damaged livers of immunotherapy recipients (Fig. 2 B).

The absence of myelomonocytic cells in the CNS of immunotherapy recipients suggested a differential pattern of chemoattractant expression between the two LCMV models. To evaluate this possibility, we isolated RNA from the brain and quantified the expression of selected chemoattractants by quantitative PCR (Q-PCR; Fig. 2 C). Consistent with the recruitment of myelomonocytic cells and T cells, mice with LCMV meningitis showed a broad range of elevated chemoattractant expression in the brain (Fig. 2 C). In contrast,

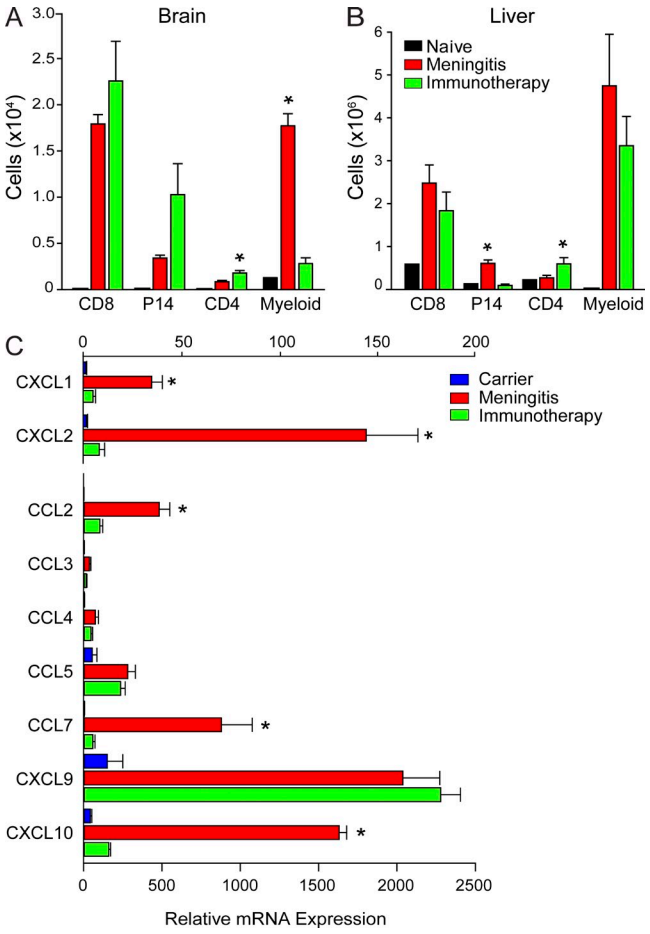

Figure 2. Tailored chemokine expression and immune infiltration is observed in the brain after immunotherapy. (A and B) The absolute number of CD8$^+$ T cells (CD45$^+$ CD8$^+$), P14 T cells (CD45$^+$ CD8$^+$ Thy1.1$^+$), CD4$^+$ T cells (CD45$^+$ CD4$^+$), and peripherally derived myeloid cells (CD45^{hi} Thy1.2$^-$ CD11b$^+$ Ly6C$^+$ and CD45^{hi} Thy1.2$^-$ CD11b$^+$ Ly6G$^+$) in the brain (A) and liver (B) was determined at day 9 after immunotherapy and compared with mice with LCMV meningitis (day 6) and naive controls (n = 4 mice per group). Asterisks indicate a statistically significant difference (*, $P < 0.05$) relative to the meningitis control group. (C) The denoted chemokines were quantified by Q-PCR using brain tissue from untreated carriers, day 9 immunotherapy recipients, or day 6 meningitis mice (n = 3 mice per group). Asterisks indicate a significant difference (*, $P < 0.05$) between the two groups. All bar graphs shown in this figure depict the mean ± SD, and data are representative of two (C) or three (A and B) independent experiments.

day 9 immunotherapy recipients had a more tailored expression pattern not observed in untreated carrier controls. Relative to mice with meningitis, immunotherapy recipients showed significantly reduced expression of CXCL1, CXCL2, CCL2, and CCL7 (Fig. 2 C), which explained the failure to recruit myelomonocytic cells. CXCL10 was also reduced in expression, whereas CXCL9 and CCL5 were elevated and likely fostered the arrival of T cells (Fig. 2 C). Collectively, these data indicate that the pattern of CNS immune surveillance is fundamentally different for mice with fatal meningitis and immunotherapy recipients.

Immunotherapy induces CD11c expression throughout the virally infected brain parenchyma

Given the absence of cytopathology in immunotherapy-treated carrier mice, we next set out to study the nature of T cell interactions in the virally infected brain parenchyma. Previous studies have shown that neurons are the primary cell population infected in the parenchyma of LCMV carrier mice (Kunz et al., 2006; Lauterbach et al., 2006). However, we postulated that microglia might also contain viral antigen, allowing them to serve as APCs during the immunotherapeutic process. To address this question, we used an mAb against the LCMV nucleoprotein (NP) to flow cytometrically quantify expression of viral antigen in microglia (Fig. 3 A). Interestingly, we observed, on average, >60% of microglia contained LCMV antigen in untreated carrier mice. These data suggested that microglia could potentially serve as APCs to antiviral T cells. To evaluate the spatial relationship between APCs and antiviral T cells after adoptive immunotherapy, we generated CD11c-YFP (Lindquist et al., 2004) carrier mice and treated these mice with antiviral memory cells that were seeded with traceable P14 CTLs expressing OFP under the actin promoter (referred to as OFP$^+$ P14 cells). We published previously that host CD11c$^+$ APCs were required for successful clearance of CNS virus after adoptive immunotherapy in carrier mice (Lauterbach et al., 2006). Consistent with this conclusion, we observed a significant increase in the parenchymal distribution of CD11c$^+$ cells 12 d after adoptive immunotherapy relative to untreated carrier controls (Fig. 3, B and C). The cells colocalized with CNS-infiltrating OFP$^+$ P14 CTLs, which were also found throughout the parenchyma of immunotherapy recipients (Fig. 3 C). These data suggested that therapeutic antiviral T cells induced CD11c expression in the virally infected brain.

Microglia convert into APCs after adoptive immunotherapy

To determine the identity and potential function of the brain-resident CD11c-YFP$^+$ cells, we performed Q-PCR and flow cytometric analyses after adoptive immunotherapy. Analysis of total brain RNA by Q-PCR revealed that CD11c expression increased significantly in expression between days 6 and 10 after immunotherapy (Fig. 4 A). This corresponded temporally with the arrival of antiviral T cells (Lauterbach et al., 2006). We reported previously that antiviral CTLs can promote recruitment of peripherally derived CD11c$^+$ APCs after adoptive immunotherapy (Lauterbach et al., 2006), but the ubiquitous distribution observed in the parenchyma of treated CD11c-YFP carrier mice suggested that brain-resident microglia might also become activated and function as APCs (Fig. 3 C). To evaluate this possibility, we flow cytometrically quantified CD11c-YFP expression in microglia extracted from the brains of treated and untreated carrier mice (Fig. 4, B and C). Relative to naive uninfected control mice, untreated LCMV carriers showed a twofold increase in the percentage of CD11c-YFP–expressing microglia (Fig. 4, B and C). These data indicate that persistent viral infection alone can result in some microglial activation. At 12–13 d

after immunotherapy, the percentage of CD11c-YFP$^+$ microglia increased significantly. On average, 80% of microglia expressed CD11c at this time point, and in some mice all microglia were CD11c-YFP$^+$. These data were consistent with the distribution of CD11c-YFP$^+$ observed on sagittal brain tissue sections (Fig. 3 C). Moreover, based on phenotypic analysis, >94% of the CD11c-YFP$^+$ cells observed in the brains of immunotherapy recipients at day 7 and 12 after immunotherapy were in fact CD45^{lo} CD11b$^+$ Ly6C$^-$ microglia and not peripherally derived myeloid cells (Fig. 5, A and B). Previous studies have used these phenotypic markers to flow cytometrically distinguish between microglia and monocytes/macrophages (Sedgwick et al., 1991; Butovsky et al., 2012; D'Agostino et al., 2012), and the meninges (which are devoid of microglia) served as control for the validity of this approach (Fig. 5 C).

Because CD11c-YFP expression was used as a surrogate for cellular activation, we next sought insights into whether microglia acquired APC-like properties in immunotherapy recipients. Analysis of MHC I and MHC II expression on CD11c$^+$ versus CD11c$^-$ microglia at day 12 revealed that both were significantly elevated on CD11c$^+$ cells (Fig. 4, D and E). In addition, a fraction of microglia from immunotherapy recipients acquired the ability to produce T cell–recruiting chemoattractants like CXCL9 and CCL5 (Fig. 4, F and G). We further assessed the activation state of CD11c-YFP$^+$ microglia by sorting these cells from day 12 immunotherapy recipients and comparing their gene expression with microglia isolated from carrier control mice using microarray analysis. This comparison revealed 931 differentially regulated genes (Fig. 6 A and see Table S2 for a complete list) between the two groups. Interestingly, antigen presentation and cellular proliferation were among the top pathways/functions expressed in microglia from day 12 immunotherapy recipients (Fig. 6, B and C; and Table S2). The prediction based on Z-score was that immunotherapy increased cellular proliferation in CD11c$^+$ microglia and simultaneously decreased activation of genes associated with organismal death (Fig. 6 B). Ingenuity Pathway Analysis (IPA) also revealed that genes associated with antigen presentation (e.g., CD74, CIITA, MHC I, MHC II, NLRC5, PSMB9, and TAP1) were highly expressed in activated microglia (Fig. 6 C), supporting their conversion into APCs. Examination of genes that intersected with our surrogate activation marker, CD11c, uncovered a complex network of differential gene expression and a direct link to STAT1 signaling (Fig. 6 D). Collectively, these data demonstrate that immunotherapy promotes a massive transformation of microglia. These cells not only contained viral antigen (Fig. 3 A), but acquired the ability to proliferate, present antigen, and recruit/interact with antiviral T cells (Figs. 4 and 6).

Microglia interact with antiviral T cells

To determine whether antiviral T cells interacted directly with CD11c$^+$ microglia during adoptive immunotherapy, we performed two-photon laser-scanning microscopy (TPLSM)

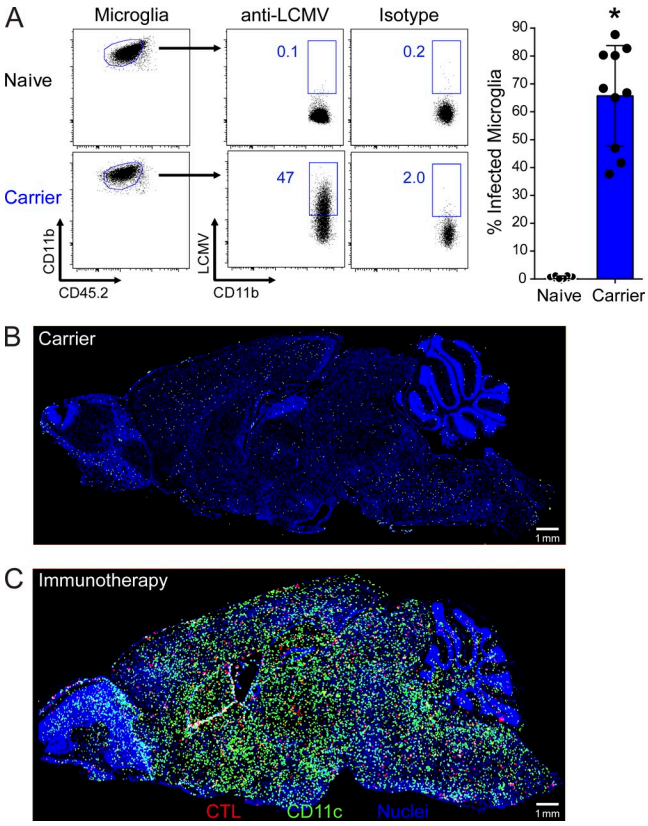

Figure 3. Distribution of viral antigen and CD11c expression in the persistently infected brain. (A) Representative flow plots show the frequency of microglia containing LCMV antigen in carrier mice versus uninfected naive controls. Microglia were identified as CD45$^{lo/int}$ Thy1.2$^-$ Gr-1$^-$ CD11b$^+$ cells. Bar graph depicts the mean ± SD, and each dot represents an individual mouse. All data from a total of four independent experiments (n = 2–3 mice per group per experiment) are graphed. The asterisk denotes a statistically significant difference (*, $P < 0.001$) between the two groups. (B and C) Representative images of sagittal brain sections are shown for CD11c-YFP$^+$ (green) carrier mice that are either untreated (B) or received adoptive immunotherapy (day 11; C) seeded with OFP$^+$ P14 CD8$^+$ T cells (red; n = 3 mice per group). Cell nuclei are shown in blue. Data are representative of three independent experiments.

to study T cell–microglia interactions in living brain tissue (Herz et al., 2012). We studied antiviral CD8$^+$ and CD4$^+$ T cell dynamics simultaneously by seeding memory donor mice with OFP$^+$ P14 cells and TFP$^+$ SMARTA cells. The latter are TCR-tg mice in which nearly all CD4$^+$ T cells recognize the LCMV glycoprotein amino acids 61–80 (Oxenius et al., 1998). Memory splenocytes containing OFP$^+$ P14 cells and TFP$^+$ SMARTA cells were adoptively transferred into CD11c-YFP$^+$ carrier mice and examined by TPLSM on day 12 (Fig. 7). Interestingly, both traceable antiviral T cell populations interacted frequently with parenchymal CD11c$^+$ cells resembling microglia (Fig. 7, A and B; and Video 1). Analysis of these dynamic interactions revealed that antiviral CD8$^+$ P14 cells tended to interact stably with CD11c$^+$ cells, whereas CD4$^+$ SMARTA cells engaged in more short duration interactions. This conclusion is supported by plots of instantaneous

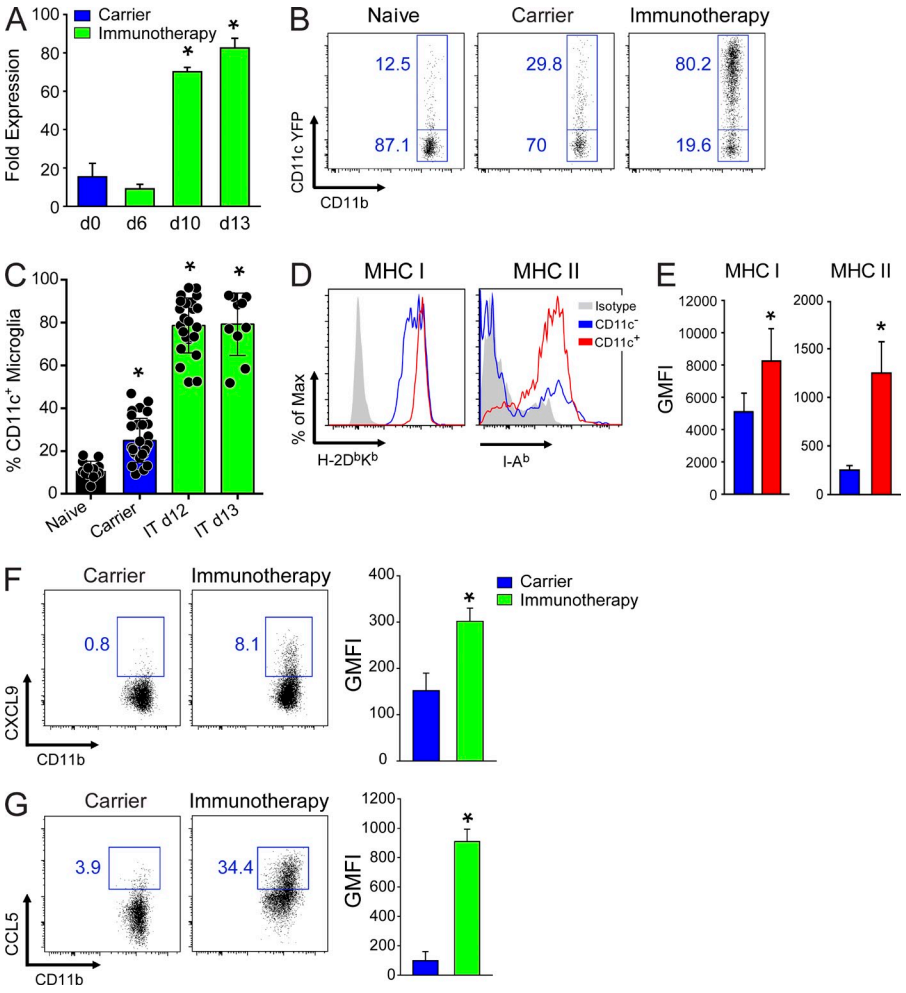

Figure 4. Microglial activation in immunotherapy recipients. (A) CD11c expression was quantified by Q-PCR using total brain RNA from untreated, day 6, day 10, and day 13 immunotherapy recipients. β-Actin was used as a reference gene to calculate normalized fold expression. The bar graph shows the mean ± SD for each group (n = 3 mice per group; representative of two independent experiments). Asterisks denote a statistically significant increase (*, $P < 0.01$) relative to untreated LCMV carrier mice. (B) Representative flow cytometric plots show the frequency of microglia (CD45$^{lo/int}$ Thy1.2$^-$ Ly6C$^-$ Ly6G$^-$ CD11b$^+$) expressing CD11c-YFP in the brains of naive, carrier, and day 12 immunotherapy mice. Boxes and associated percentages denote the frequency of CD11c-YFP$^+$ and CD11c-YFP$^-$ microglia. (C) Bar graph shows the frequency of CD11c-YFP$^+$ microglia (mean ± SD) in naive, carrier, and immunotherapy (IT) recipients at days 12 and 13. All data are shown from a combination of 19 independent experiments (n = 1–4 mice per group per experiment; *, $P < 0.05$). (D and E) Representative histograms (D) and bar graphs (E) show the expression of MHC I (H-D^{b}K^b) and MHC II (I-A^b) on CD11c-YFP$^+$ and CD11c-YFP$^-$ microglia at day 12 after immunotherapy. Isotype control antibody staining is shown in gray on the histograms. Microglia were gated as described in B. Bar graphs show the geometric mean fluorescent intensity (GMFI) represented as mean ± SD (n = 5 mice per group). Data are representative of three independent experiments, and asterisks denote statistical significance (*, $P < 0.05$). (F and G) Representative histograms and bar graphs depict the expression of CXCL9 (F) and CCL5 (G) by microglia from carriers and day 12 immunotherapy recipients. Microglia were gated as described in B. Boxes denote the frequency of chemokine-expressing cells. Bar graphs show the mean ± SD. GMFI is shown (n = 4–5 mice per group; three independent experiments; *, $P < 0.05$).

T cell track velocities over time, demonstrating that antiviral CD8$^+$ T cells often decelerated to <2 μm/min and stably arrested after engagement (Fig. 7 B and Video 1). In contrast, antiviral CD4$^+$ T cells associated with CD11c$^+$ cells for similar amounts of time but were highly motile during these interactions. This was confirmed by quantification of mean T cell track velocities, which showed that antiviral CD8$^+$ T cells were significantly slower than CD4$^+$ T cells (Fig. 7 C). Despite this difference in velocity, the amount of time spent interacting with parenchymal CD11c$^+$ cells (either stably or dynamically) was identical for antiviral CD8$^+$ and CD4$^+$ T cells (Fig. 7 D). Greater than 40% of all antiviral T cells examined by TPLSM spent >8 min interacting with CD11c$^+$ cells. These data indicate that antiviral T cells interact directly with CD11c$^+$ cells during adoptive immunotherapy, with CD8$^+$ T cells preferring to engage stably and CD4$^+$ T cells doing so in a dynamic manner.

Because antiviral CD8$^+$ T cells interacted stably with microglia, we further explored the MHC I dependence of these engagements. CD8$^+$ P14 cells that contacted CD11c$^+$ microglia showed reduced mean track velocities and meandering factors relative to those that did not (Fig. 8 A). This suggested that the antiviral T cells spent more time interacting with microglia than other brain targets, an assumption supported by the elevated arrest coefficients for T cells that contacted microglia (Fig. 8 A). To determine whether these interactions were influenced by MHC I, the same T cell motility parameters were quantified in the presence of an MHC I blocking antibody. Inhibition of MHC I interactions increased mean track velocities/meandering factors and decreased arrest coefficients for CD8$^+$ P14 cells that contacted CD11c$^+$ microglia in immunotherapy recipients (Fig. 8 B). These data demonstrate that the interactions between antiviral CD8$^+$ T cells and microglia are MHC I dependent.

Antiviral T cells induce IFNγ signaling in CD11c$^+$ microglia

Given that therapeutic antiviral T cells interacted directly with CD11c$^+$ microglia, we next set out to determine whether

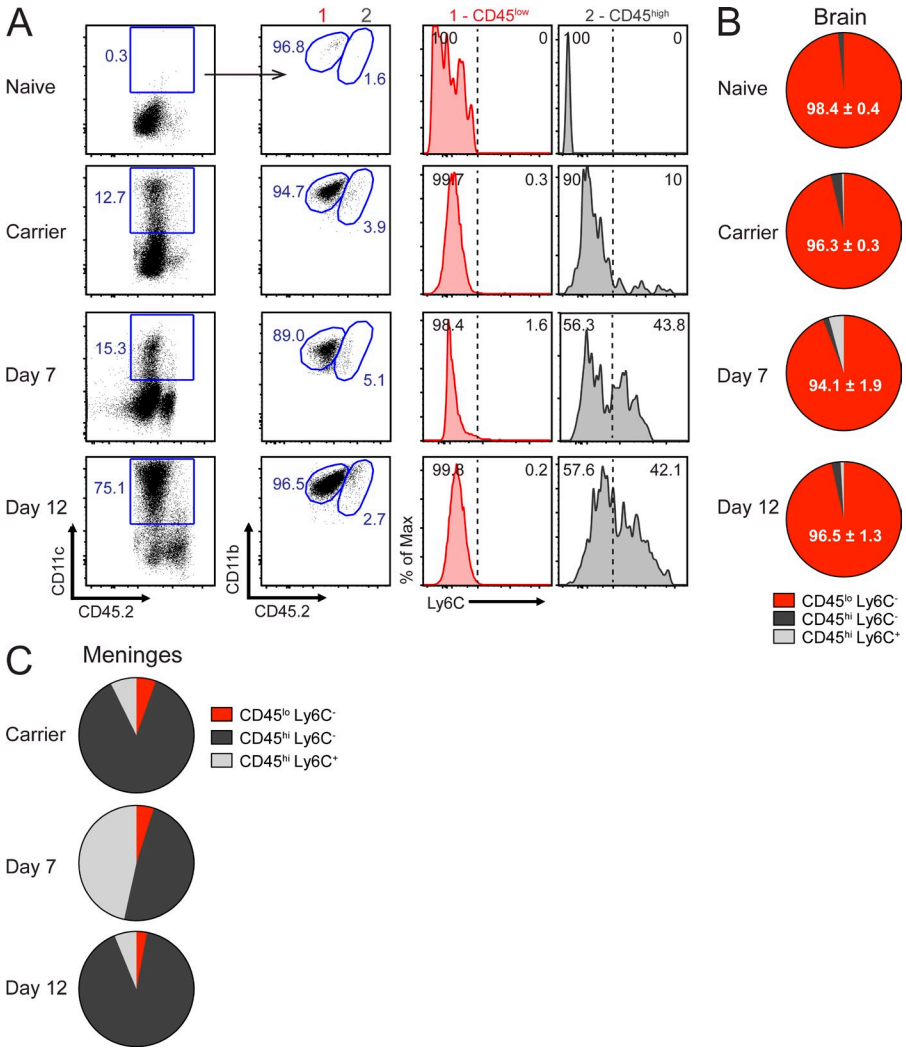

Figure 5. Derivation of CD11c$^+$ myeloid cells after immunotherapy. (A) Representative flow cytometric plots show the gating strategy used to identify CD11c$^+$ Thy1.2$^-$ myeloid cells in the brain and meninges of naive, carrier, and immunotherapy mice ($n = 3$ mice per group). CNS-infiltrating leukocytes were analyzed for expression of CD45.2, CD11b, and Ly6C. Resident microglia (gate 1) were identified as CD45^{lo} Ly6C$^-$, whereas peripherally derived myeloid cells (gate 2) were CD45^{hi} Ly6C$^{+/-}$. (B and C) Pie graphs depict the percentage of CD11c$^+$ cells in the brain (B) and meninges (C) determined to be either microglia or peripherally derived myeloid cells. The frequencies of CD11c$^+$ microglia (mean ± SD) are provided in B. Data are representative of two independent experiments.

these interactions were functional and induced antiviral signaling. Previous studies have shown that IFN-γ production by antiviral T cells is required for successful viral clearance after adoptive immunotherapy (Tishon et al., 1995). Therefore, we examined the brains of immunotherapy recipients for evidence of IFNγ production and downstream signaling in CD11c$^+$ microglia. At day 12 after immunotherapy, a significant increase in IFNγ mRNA expression was observed relative to naive and untreated carrier controls (not depicted). This coincided with the arrival of antiviral CD8$^+$ and CD4$^+$ T cells expressing IFNγ (Fig. 9, A and B). Therapeutic administration of memory T cells from IFNγ-YFP reporter mice revealed that >50% of donor-derived CD8$^+$ and CD4$^+$ T cells in the brains of day 12 immunotherapy recipients were IFNγ-YFP$^+$. No YFP was observed in memory donor T cells before adoptive transfer unless stimulated ex vivo with cognate peptide (Fig. 9 A and not depicted). In addition, analysis of splenocytes from IFNγ-YFP mice 8 d after an acute LCMV infection revealed that YFP expression localized exclusively to IFNγ$^+$ LCMV-peptide stimulated CD8$^+$ ($GP_{33–41}$, $NP_{396–404}$, $GP_{276–286}$, and $NP_{205–212}$) and CD4$^+$ ($GP_{61–80}$) T cells (not depicted). These data suggest that the majority of donor-derived T cells that enter the brain are LCMV specific.

To determine whether CD11c$^+$ microglia responded to donor T cell–derived IFNγ, we performed adoptive immunotherapy using memory T cells from IFNγ-deficient mice. As a measure of IFNγ signaling, we quantified MHC II expression (an IFNγ inducible gene) on CD11c-YFP$^+$ microglia at day 12 after immunotherapy. When compared with carrier mice treated with wild-type cells, a significant reduction in MHC II (but not MHC I) expression was observed on CD11c-YFP$^+$ microglia after transfer of IFNγ$^{-/-}$ T cells (Fig. 9 C) but not TNF$^{-/-}$ T cells (not depicted). This reduction could not be explained by a difference in T cell homing to the CNS, as an equivalent number of wild-type and IFNγ$^{-/-}$ T cells were detected in the brain at day 12 after immunotherapy (not depicted). To provide further evidence for IFNγ-mediated signaling in CD11c$^+$ microglia, we quantified phospho-STAT1 expression by immunohistochemistry (Fig. 9, D–F). In untreated LCMV carrier mice, the brain parenchyma contained very few CD11c-YFP$^+$ cells

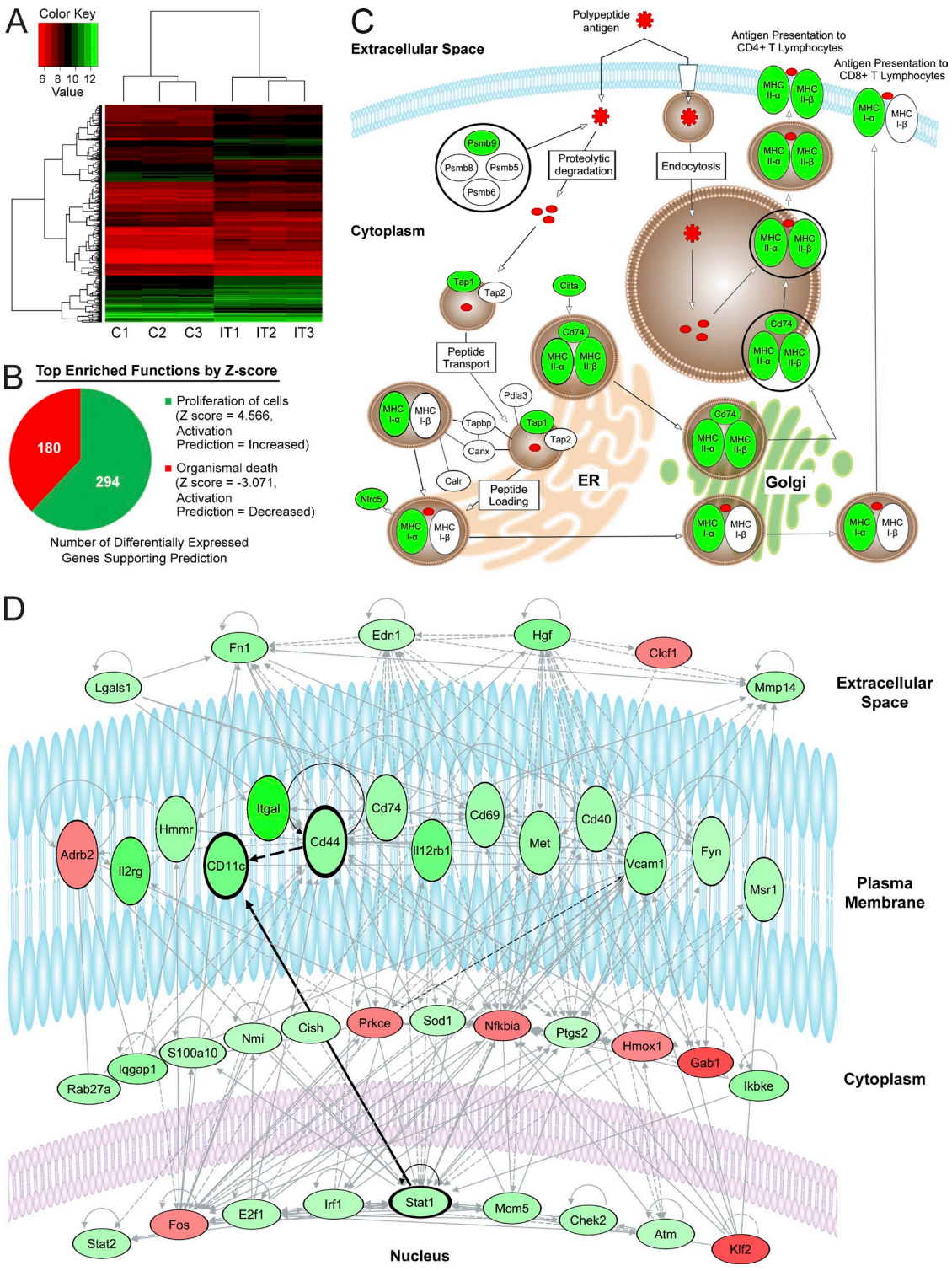

Figure 6. Immunotherapy induces differential gene expression and antigen-presenting machinery in CD11c⁺ microglia. (A) The heat map depicts differential gene expression (y axis) in microglia (CD45^{lo} 7-AAD^{-} Thy1.2^{-} Gr1^{-} CD11b^{+} CD39^{+} CX3CR1-GFP^{+} [carrier] or CD11c-YFP^{-} [immunotherapy]) flow cytometrically sorted from the brains of day 12 immunotherapy (IT) recipients versus untreated carrier controls (C; x axis; $n = 3$ mice per group). See corresponding Table S2. (B) IPA software was used to identify enriched functions and pathways from the microarray data. A complete list is provided in Table S2. The pie graph depicts the number of differentially regulated genes that intersect with two enriched IPA functions: proliferation of cells (green) and organismal death (red). The corresponding activation prediction based on Z-score is also provided. (C and D) IPA software was used to generate the interacting networks of genes associated with antigen presentation (C) and CD11c expression (D). Genes that were up-regulated in microglia from day 12 immunotherapy recipients are shown in shades of green, whereas down-regulated genes are shades of red. Data are derived from a single experiment.

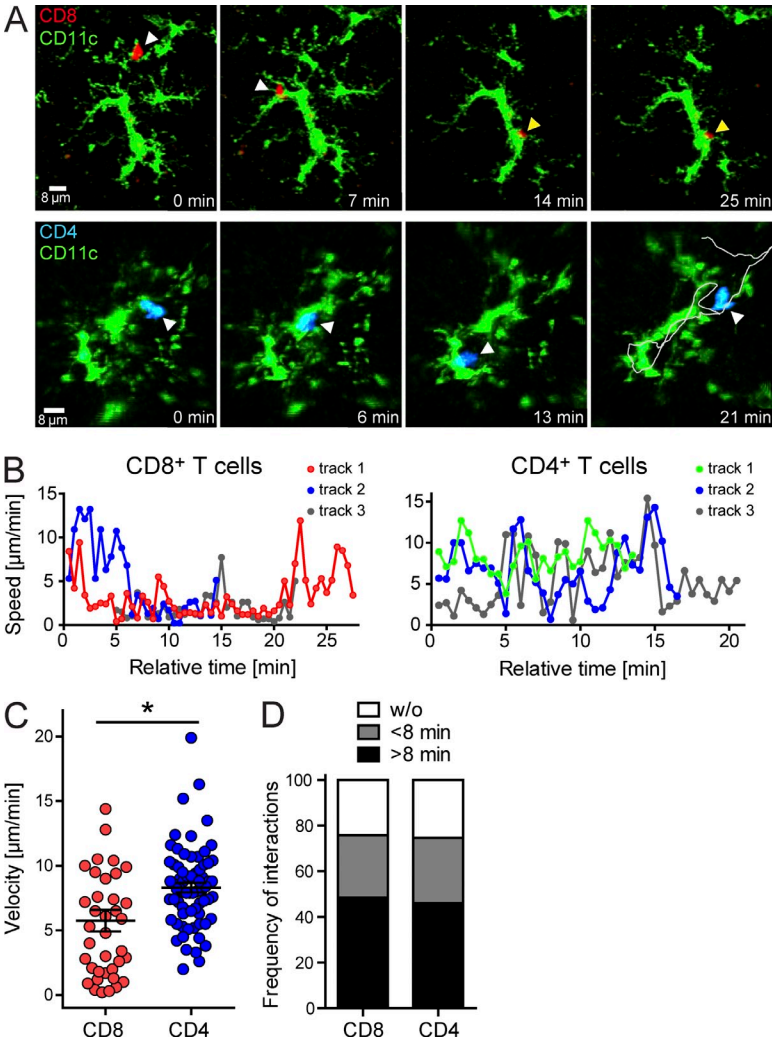

Figure 7. Antiviral CD8⁺ and CD4⁺ T cell interactions with CD11c⁺ microglia after immunotherapy. (A) Two-photon imaging experiments were performed in CD11c-YFP⁺ carrier mice 12 d after adoptive transfer of memory splenocytes containing OFP⁺ CD8⁺ P14 (red) and TFP⁺ CD4⁺ SMARTA (blue) memory T cells. Representative maximal projections extracted from 3D time lapses show interactions between CD11c-YFP⁺ microglia (green) and P14 (top) or SMARTA (bottom) cells over a 20–25-min time period. Arrowheads denote the position of the antiviral T cells at the different time points. White arrowheads indicate that the T cell was in motion at the denoted time point, whereas yellow indicates stable T cell arrest while in contact with the CD11c-YFP⁺ cell. The gray line depicted on the final CD4 T cell image shows the entire path taken by the cell while interacting with the CD11c-YFP⁺ target. (B) Instantaneous velocities were plotted versus time for individual CD8⁺ P14 and CD4⁺ SMARTA T cells interacting with CD11c-YFP⁺ microglia in the brain parenchyma at day 12 after immunotherapy. Each track represents a single T cell. Instantaneous velocities of <2 µm/min signify stable arrest. (C) The scatter plot shows the mean track velocities for individual CD8⁺ P14 and CD4⁺ SMARTA T cells interacting with CD11c-YFP⁺ microglia. Each dot represents an individual T cell. Horizontal black lines denote the mean ± SD of the groups. *, $P < 0.05$. (D) The bar graph depicts the proportional duration of time (none, <8 min, and >8 min) individual CD8⁺ P14 and CD4⁺ SMARTA T cells spent interacting with CD11c-YFP⁺ cells. All data in this figure are representative of two independent experiments ($n = 3$ mice per group).

and was almost completely devoid of pSTAT1 staining (Fig. 9 D). In contrast, a marked increase in parenchymal pSTAT1 staining was observed in day 12 immunotherapy recipients, and some of this staining overlapped with CD11c-YFP⁺ cells, as well as NeuN⁺ neurons (Fig. 9, D and E). Quantitative analyses of individual cells revealed that ∼13% of parenchymal CD11c-YFP⁺ cells and ∼7% of NeuN⁺ neurons were pSTAT1⁺ after adoptive immunotherapy (Fig. 9, E and F). Collectively, these data indicate that T cell–derived IFNγ induces antiviral signaling in CD11c⁺ microglia.

Microglia proliferate and are noncytopathically purged of virus

Antiviral T cell interactions with infected APCs and neurons in brain parenchyma can give rise to immunopathology (Merkler et al., 2006; Kreutzfeldt et al., 2013). Effector T cells possess lytic effector molecules like granzymes and perforin that are known to induce apoptosis (Kägi et al., 1996). Indeed, the majority of P14 CTLs (∼65%) extracted from the brains of day 12 immunotherapy recipients expressed granzyme B, which was only modestly reduced when compared with CTLs obtained from day 6 meningitis mice (the positive control for this experiment; Fig. 10 A). Interestingly, despite the presence of granzyme B–expressing CTLs, no evidence of increased apoptosis was observed in CD11c-YFP⁺ microglia from day 12 (Fig. 10 B) or day 30 (not depicted) immunotherapy recipients relative to untreated carrier control mice. Instead, >40% of microglia incorporated i.p. injected BrdU, indicating that they had proliferated (Fig. 10 C). These data are consistent with the microarray data, which predicted an increase in cellular proliferation and a decrease in organismal death (Fig. 6 B). Moreover, nearly all microglia were purged of virus over time (Fig. 10 D). This clearance process was dependent on IFNγ, as LCMV was not purged from microglia when IFNγ$^{-/-}$ T cells were used (Fig. 10 E and not depicted). These data suggest that infected microglia are cleared noncytopathically despite being engaged by antiviral T cells possessing granzymes.

DISCUSSION

The virally infected CNS poses a considerable challenge to the immune system because it is relatively intolerant of

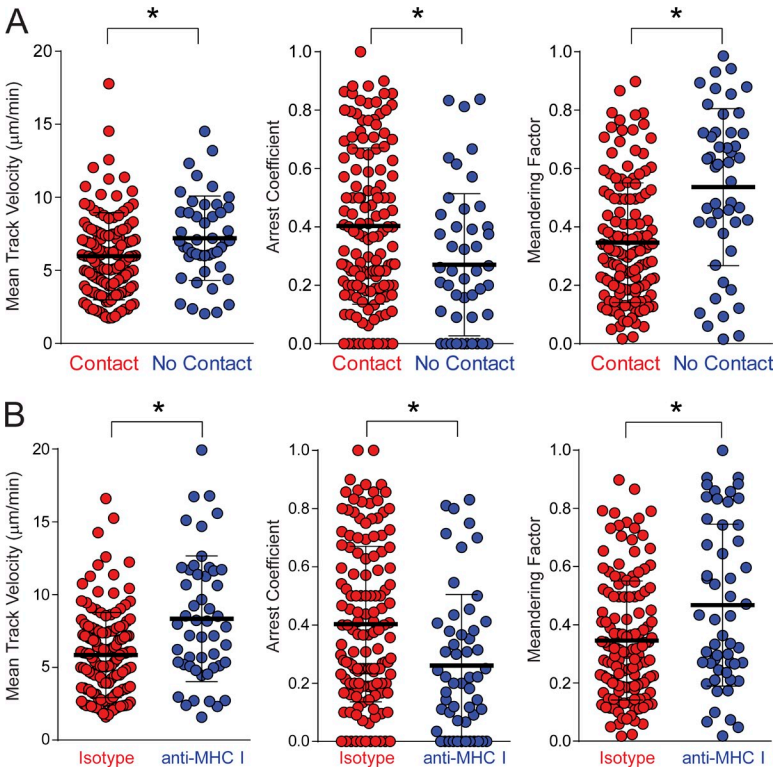

Figure 8. Virus-specific CD8⁺ T cell interactions with CD11c⁺ microglia are MHC I dependent. (A) Two-photon imaging experiments were performed in CD11c-YFP⁺ carrier mice 12 d after adoptive transfer of memory splenocytes containing OFP⁺ CD8⁺ P14 T cells. Mean track velocities, arrest coefficients, and meandering factors are shown for OFP⁺ P14 T cells that either did or did not establish contact with CD11c-YFP⁺ microglia in time lapses examined over a 1-h time interval (n = 4 mice per group). (B) Two-photon analyses of OFP⁺ P14 T cells interacting with CD11c-YFP⁺ cells were performed on brain slices incubated with MHC I blocking or isotype control antibodies at day 12 after immunotherapy (n = 4 mice per group). Motility parameters are shown for P14 T cells that contacted CD11c⁺ microglia for >30 s during the length of the track. All data in this figure are representative of two independent experiments. Colored dots represent individual T cells, and the mean ± SD for each group is depicted with horizontal black lines. *, $P < 0.05$.

immunopathology. Thus, it is important to explore the nature of benign immune interactions within this compartment, particularly those that result in viral clearance. Although antiviral T cells can promote undesirable immunopathology (Kägi et al., 1996), they do possess the capacity to purge viruses noncytopathically (Guidotti et al., 1999b; Guidotti and Chisari, 2001). In this study, we sought novel insights into the therapeutic removal of a persistent virus from the brain. We uncovered that microglia in addition to neurons contained LCMV in mice persistently infected from birth (LCMV carrier). Because microglia can serve as APCs (Nayak et al., 2014), their infection in this model opened the possibility of CNS immunopathology after T cell engagement. Interestingly, however, therapeutic antiviral T cells not only achieved clearance of the brain parenchyma, but did so in the absence of cellular apoptosis or vascular leakage. This was achieved through a tailored response that involved selective recruitment of antiviral T cells but not pathogenic myelomonocytic cells. We also observed that therapeutic T cells promoted the conversion of nearly all brain-resident microglia into CD11c$^+$ APCs with the capacity to produce chemokines, present antigen, proliferate, and interact directly with antiviral T cells. This program was induced in part via IFNγ signaling, which was evident in CD11c$^+$ microglia after adoptive immunotherapy. Even more impressive was the fact that despite phenotypic and functional conversion into APCs, microglia were cleansed by T cells without evidence of apoptosis. These data indicate that antiviral T cells can interact with the infected brain parenchyma in a benign manner and that noncytopathic removal of a virus from this compartment is an attainable therapeutic outcome.

Previous examination of LCMV carrier mice uncovered that neurons are a primary target of the virus (Mims, 1966; Rodriguez et al., 1983; Fazakerley et al., 1991), and it was postulated that these cells were cleared in an MHC I–independent manner because of their failure to display peptide–MHC I complexes (Joly et al., 1991; Joly and Oldstone, 1992). Using a more sensitive approach, our experiments have revealed that neurons are not the only cell population that contains LCMV antigen in the carrier brain. The majority of microglia also harbored detectable levels of LCMV and thus could potentially serve as antigen presenters to infiltrating antiviral T cells. This is an important observation because microglia are known to serve as APCs in models of infection and autoimmunity (McMahon et al., 2005; John et al., 2011; D'Agostino et al., 2012). Moreover, antiviral cytokines released at the immunological synapse between T cells and infected microglia could potentially spill over onto adjacently infected neurons, resulting in bystander clearance in an MHC I–independent manner. Studies of viral clearance in the infected liver have provided precedence for this mode of clearance (Guidotti et al., 1999a; Guidotti and Chisari, 2001). In addition, a recent in vitro study demonstrated that IFNγ release by T cells at the immunological synapse can result in STAT1 signaling in adjacent nonengaged cells, providing support for the concept of cytokine spillover (Sanderson et al., 2012).

Given the abundance of parenchymal targets in the LCMV carrier brain, we used sensitive measures of immunopathology to determine whether therapeutic administration of antiviral T cells had any negative impact in the CNS.

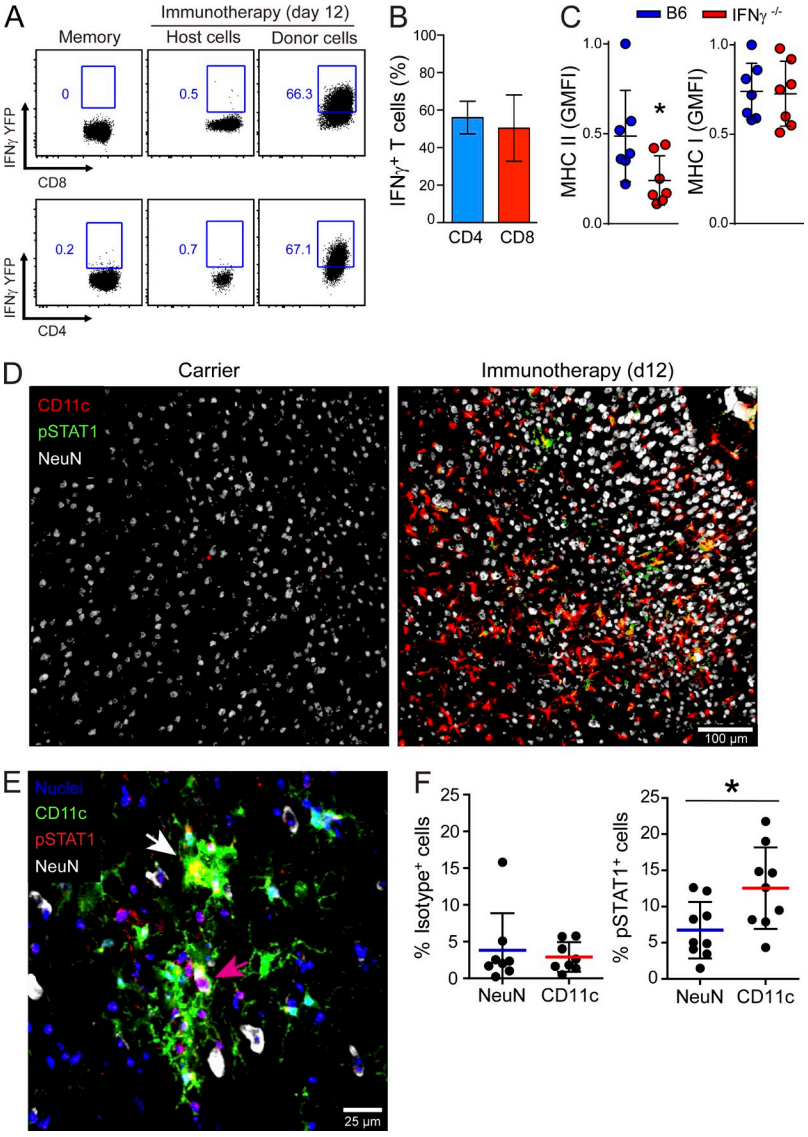

Figure 9. Antiviral T cells induce IFNγ-dependent signaling in CD11c⁺ microglia. (A) Representative FACs plots show IFNγ-YFP expression in host versus donor-derived CD8⁺ and CD4⁺ T cells extracted from the brain at day 12 after immunotherapy (n = 6 mice per group; three independent experiments). As a control, expression in memory donor cells before transfer into carrier mice is also shown. Blue boxes denote the percentage of YFP-expressing T cells. Gated on CD45⁺ Thy1.2⁺ CD8⁺ or CD4⁺ cells. (B) The bar graph shows the percentage (mean ± SD) of donor-derived IFNγ-YFP⁺ CD8⁺ or CD4⁺ T cells in the brains of day 12 immunotherapy recipients. (C) Dot plots depict the normalized expression of MHC I and II on CD11c-YFP⁺ microglia 12 d after administration of memory splenocytes from B6 or IFNγ$^{-/-}$ mice. Microglia were identified as CD45$^{lo/int}$ Thy1.2^{-} Ly6C^{-} Ly6G^{-} CD11b⁺ CD11c-YFP⁺ cells. Each dot represents an individual mouse (n = 7 mice per group; three independent experiments; *, $P < 0.05$), and horizontal black lines denote the mean ± SD of the groups. (D) Representative images show the distribution of CD11c-YFP, pSTAT1, and NeuN in the brain parenchyma of LCMV carrier and day 12 immunotherapy recipients. Note the increased appearance of pSTAT1⁺ CD11c⁺ cells (yellow) in the immunotherapy recipients. (E and F) Nuclear pSTAT1 staining was quantified by analyzing the parenchyma of brain tissue sections stained with DAPI (nuclei), CD11c-YFP, NeuN, and pSTAT1 (E). The white arrow denotes a CD11c-YFP⁺ cell with nuclear pSTAT1 staining (appears yellow). A NeuN⁺ neuron with nuclear pSTAT1 staining (appears pink) is highlighted by a pink arrow. Dots plots show the frequency of pSTAT1⁺ neurons or CD11c-YFP⁺ cells that were positive for nuclear anti-pSTAT1 staining. An isotype control antibody was used to determine background signal. Horizontal lines depict the mean and SD of the groups. Each dot represents the frequency of pSTAT1⁺ NeuN⁺ or pSTAT1⁺ CD11c⁺ cells per 635-µm² tissue area within the cerebral cortex (n = 4–5 mice per group; two independent experiments; *, $P < 0.05$).

Antiviral T cells do indeed have the capacity to induce severe immunopathology in the LCMV-infected brain. This is exemplified in adult mice infected intracerebrally with LCMV, which induces fatal immune-mediated meningitis (McGavern et al., 2002a,b; Kim et al., 2009). Interestingly, carrier mice receiving adoptive immunotherapy showed no significant increase in parenchymal apoptosis or vascular leakage despite having a comparable number of brain-infiltrating CTLs to mice with meningitis. It is important to note that this noncytopathic pattern of clearance was most notable in the brain, as the livers of carrier mice receiving antiviral T cells showed evidence of severe immunopathology. These data indicate that the CNS has the capacity to uniquely regulate antiviral T cells despite widespread viral infection of the parenchyma and meninges. LCMV carrier mice contain viral antigen in the same meningeal target cells as mice with acute meningitis (unpublished data), yet they do not develop neurological symptoms or immunopathology.

To better understand this process, we examined the composition of the CNS infiltrate in carrier mice that received immunotherapy. The infiltrate composition is critical because we demonstrated previously in mice with LCMV meningitis that antiviral CD8⁺ T cells can promote the recruitment of innate myelomonocytic cells, which severely disrupt CNS vascular integrity through synchronous extravasation (Kim et al., 2009; Kang and McGavern, 2010). CD8⁺ T cells accomplish this through the release of myelomonocytic cell–recruiting chemoattractants (Kim et al., 2009). In contrast to mice with meningitis, we observed that the brains of immunotherapy recipients were completely devoid of myelomonocytic cells, and this was explained mechanistically by a narrow chemoattractant expression profile. Only two of the chemoattractants quantified (CCL5 and CXCL9) were notably elevated in carrier mice after transfer of antiviral T cells. Mice with acute meningitis showed a broad spectrum of chemoattractant expression that likely favored recruitment of a more diverse

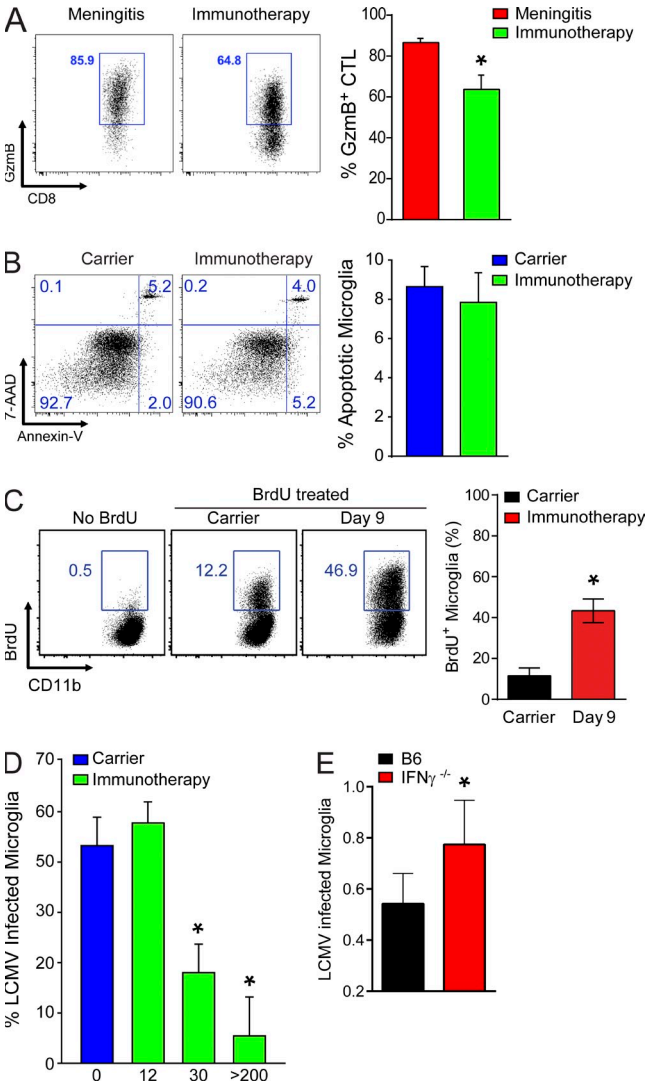

Figure 10. Antiviral T cells noncytopathically clear virus from microglia. (A) Representative FACs plots show the frequency of granzyme B$^+$ CD8$^+$ P14 T cells (blue boxes) in the brains of day 12 immunotherapy recipients. Day 6 LCMV meningitis mice were used as a positive control for this experiment. FACs plots are gated on CD45$^+$ CD8$^+$ Thy1.1$^+$ cells. The bar graph shows the mean ± SD frequency of granzyme B$^+$ antiviral CTLs (n = 4 mice per group; two independent experiments; *, $P < 0.05$). (B) Representative FACs plots show the frequency of Annexin V$^+$ and 7-AAD$^+$ microglia at day 12 after immunotherapy. Plots are gated on CD45$^{lo/int}$ Thy1.2$^-$ Gr1$^-$ CD11b$^+$ cells. The bar graph shows the frequency (mean ± SD) of Annexin V$^+$ microglia (n = 3 mice per group; three independent experiments). (C) Representative FACs plots show BrdU expression in microglia (CD45.2^{lo} Thy1.2$^-$ Ly6C$^-$ Ly6G$^-$ CD11b$^+$) from carrier mice and day 9 immunotherapy recipients. A plot from a control mouse that did not receive BrdU is also shown. The frequencies (mean ± SD) of BrdU$^+$ microglia are provided in the bar graph (n = 4 mice per group; three independent experiments; *, $P < 0.05$). (D) The frequency of LCMV$^+$ microglia was determined flow cytometrically at the denoted time points after immunotherapy and compared with untreated carrier mice. Data are plotted as mean ± SD (n = 3 mice per group; two independent experiments; *, $P < 0.05$). (E) The normalized fraction of LCMV$^+$ microglia was calculated at day 30 after immunotherapy for mice that received B6 or IFN$\gamma^{-/-}$ memory cells. Data are plotted as mean ± SD (n = 7 mice per group from two independent experiments; *, $P < 0.05$).

CNS immune infiltrate. One possible explanation for this observation is the difference in IFN-I levels in mice with an acute versus a chronic LCMV infection. Acute LCMV infection induces a robust IFN-I response that is responsible for nearly all gene expression in the infected brain (Nayak et al., 2013). This innate program is so important in shaping pathogenic CNS immune activity that deficiency in IFN-I signaling completely prevents fatal LCMV meningitis (Müller et al., 1994; Sandberg et al., 1994). In contrast, LCMV carrier mice have grown up with the virus from birth and therefore have very low levels of IFN-I in circulation despite being highly viremic (Bukowski et al., 1983). Adoptive transfer of antiviral T cells into mice with low IFN-I could favor the induction of a more tailored chemokine response driven by type 2 IFN, whereas abundant release of both IFN types in mice with acute meningitis may trigger a broader response.

One of the key findings in our study was the nature and consequence of antiviral T cell interactions in the persistently infected brain parenchyma. The CNS meninges and choroid plexus are inhabited by peripherally derived CD11c$^+$ APCs that bear some resemblance to splenic DCs (Anandasabapathy et al., 2011). Studies have also demonstrated that peripherally derived DCs can enter the brain during states of inflammation (Fischer et al., 2000; Karman et al., 2004; Lauterbach et al., 2006; John et al., 2011; D'Agostino et al., 2012). In fact, we showed previously that successful viral clearance after adoptive immunotherapy in LCMV carrier mice requires T cell–DC interactions (Lauterbach et al., 2006). However, DCs are not the only APCs that express CD11c$^+$. Microglia have been shown to up-regulate CD11c after activation both in vitro (Santambrogio et al., 2001) and in vivo (Bulloch et al., 2008). Consistent with this potential, we observed that therapeutic antiviral T cells induced most brain-resident microglia to up-regulate CD11c, proliferate, and convert into APCs with the enhanced ability to present antigen and produce T cell–recruiting chemoattractants like CCL5 and CXCL9. In fact, the vast majority of CD11c$^+$ APCs extracted from the brains of immunotherapy recipients were microglia, and our microarray data revealed differential gene expression in these cells consistent with a marked cellular transformation. A program consisting of at least 931 differentially regulated genes was induced, with notable features including enhanced antigen presentation machinery, entrance into cell cycle, and potential resistance to cell death, among others (see Table S2 for a complete list). We postulate that these properties endowed microglia with the ability to withstand the onslaught of antiviral T cells.

The mechanism of microglia activation after antiviral T cell infiltration was dependent in part on T cell–derived IFNγ, a cytokine required for successful viral clearance in immunotherapy recipients (Tishon et al., 1995). Evidence of downstream signaling (pSTAT1) was detected in parenchymal

$CD11c^+$ microglia, which is consistent with the link between STAT1 signaling and CD11c expression revealed in our pathway analysis of the microarray data. In fact, CD11c intersected with a network of 40 differentially regulated genes in microglia extracted from immunotherapy recipients (Fig. 6 D). Expression of these genes would equip microglia with a range of functions, including protection from free radicals (SOD1), cell cycle progression (E2F1 and MCM5), adhesion (VCAM1, ITGAL, and CD44), increased activation (CD40), metalloproteinase activity (MMP14), IL-12 signaling (IL12RB1), scavenging (MSR1), signal transduction (STAT1 and STAT2), an ability to induce vasoconstriction (EDN1), etc. The up-regulation of STAT1 and STAT2 suggested a role for IFN signaling in this microglial activation program. This assumption was supported by data showing that adoptive transfer of IFNγ-deficient antiviral T cells resulted in significantly reduced MHC II expression on microglia and no viral clearance. This is consistent with a previous study showing that stereotactic injection of IFNγ into the brain induced up-regulation of MHC II on $CD11c^+$ microglia (Gottfried-Blackmore et al., 2009). Microglia activation may also depend on other cytokines like GM-CSF. For example, microglia stimulated in vitro with GM-CSF were shown to up-regulate $CD11c^+$ and acquire a DC-like phenotype (Santambrogio et al., 2001), and pathway analysis revealed evidence of GM-CSF signaling in microglia after immunotherapy (Table S2). Thus, complete activation and differentiation of microglia in the virally infected brain may require a combination of signals.

At the dynamic level, our TPM experiments uncovered that antiviral $CD8^+$ and $CD4^+$ T cells interacted differently with $CD11c^+$ microglia. $CD8^+$ T cells stably engaged microglia in an MHC I–dependent manner, whereas $CD4^+$ T cells preferred highly dynamic associations without arresting. This could be caused by a difference in the relative abundance of cognate peptide–MHC I versus MHC II complexes expressed on the surface of microglia in LCMV carrier mice. Low peptide–MHC II in the presence of chemokine release may override the TCR-induced stop signal in $CD4^+$ T cells, fostering an association with microglia but not full arrest (Bromley et al., 2000). It has nevertheless been shown that even short-duration interactions like these can result in T cell signaling (Friedman et al., 2010). Even more interesting is the fact that despite stable engagement by antiviral CTLs, microglia were purged of virus without evidence of apoptosis. In fact, our microarray and BrdU studies demonstrated that immunotherapy induced significant microglia proliferation, which may render these cells less susceptible to CTL-induced cell death. A previous study demonstrated that CTLs can achieve noncytolytic clearance of HSV-1–infected sensory neurons via granzyme B–mediated degradation of an essential viral protein (Knickelbein et al., 2008). Antiviral cytokines such as IFNγ and TNF have also been shown to facilitate noncytopathic viral clearance (Guidotti and Chisari, 2001), and both cytokines are required for the resolution of a persistent LCMV infection after adoptive immunotherapy (Tishon et al., 1995; Lauterbach et al., 2006). However, it is important to emphasize that the sole reliance on noncytopathic viral clearance mechanisms is unique to the CNS in carrier mice. Peripheral tissues such as the liver experience significant immunopathology after adoptive immunotherapy. Further studies are required to identify the mechanism that prevents the induction of apoptosis in $LCMV^+$ microglia engaged by CTLs. One possibility is expression of serine protease inhibitors that block granzyme B–induced cell death. These inhibitors are used by CTLs, for example, to prevent self-inflicted injury (Zhang et al., 2006), and several serine protease inhibitors were up-regulated in microglia from immunotherapy mice (Table S2). Another possibility is the expression of immunoregulatory molecules that uniquely shape the activity of antiviral T cells operating in the CNS parenchyma (Suvas et al., 2006).

In conclusion, our findings provide some instruction about the mechanisms underlying the noncytopathic removal of a persistent virus from the CNS. Neurons and fully activated microglia can be purged of virus through the selective recruitment of therapeutic antiviral T cells in the absence of pathogenic myelomonocytic cells. These data indicate that T cell activity in the virally infected brain is not inherently pathogenic. Other variables influence the pathogenicity of immune reactions in this specialized compartment. Great progress has been made in the development and successful implementation of adoptive immunotherapies to treat peripheral viral infections in humans. Although additional challenges lie ahead, it should be possible to remove neurotropic viruses from the human brain using this approach. One key to achieving noncytopathic clearance may be to ensure that antiviral T cells operate alone in this specialized compartment. This will require more information about the rules governing pathogenic versus nonpathogenic T cell activity in the infected CNS.

MATERIALS AND METHODS

Mice. C57BL/6J (B6), B6.129S7-Ifngtm1Ts/J ($IFN\gamma^{-/-}$), B6.129S-Tnftm1Gkl/J ($TNF^{-/-}$), and B6.129S4-Ifngtm3.1Lky/J (IFNγ-YFP) mice were purchased from The Jackson Laboratory. CX3CR1-GFP, actin-OFP^+, actin-TFP^+, $Thy1.1^+$ P14, OFP^+ P14, TFP^+ SMARTA, and CD11c-YFP^+ mice (all on a pure B6 background) were bred and maintained under specific pathogen–free conditions at the National Institutes of Health (NIH). CD11c-YFP^+ mice were provided by M. Nussenzweig (The Rockefeller University, New York, NY; Lindquist et al., 2004). Actin-OFP^+ and actin-TFP^+ were generated at the NIH as described previously (Gossa et al., 2014). All animal experiments were conducted in accordance with the guidelines set forth by the NIH Animal Care and Use Committee.

Virus infections. The Armstrong (Arm) 53b strain of LCMV was propagated and maintained on BHK-21 cells. To generate an initial colony of LCMV carriers, newborn mice were infected intracranially (i.c.) with 10^3 PFU of LCMV Arm within 24 h of birth. The carrier colony was then maintained by breeding adult persistently infected female mice with uninfected or persistently infected male mice. All offspring were confirmed to be persistently infected carriers by performing serum plaque assays on Vero cells. CD11c-YFP^+ carriers were generated by mating B6 carrier females with uninfected homozygous male CD11c-YFP mice. All resultant F1 mice were used for experimentation. LCMV meningitis was induced by infecting adult (6–8 wk old) B6 mice i.c. with 10^3 PFU of LCMV Arm.

Adoptive transfers. Memory donor mice for adoptive immunotherapy were generated by infecting mice i.p. with 10^5 PFU of LCMV Arm, which is completely cleared from all tissues within 8–10 d. Splenocytes were harvested

from LCMV immune mice at >45 d after infection. To perform adoptive immunotherapy, 2×10^7 splenocytes containing LCMV-specific memory $CD8^+$ and $CD4^+$ T cells against all known epitopes in B6 mice (Masopust et al., 2007; Dow et al., 2008) were injected i.p. into recipient LCMV carrier mice. For experiments involving tagged $CD8^+$ P14 or $CD4^+$ SMARTA T cells, the respective populations were purified from the spleens of naive tg mice using negative selection kits (STEMCELL Technologies). Naive donor mice were then seeded i.v. with 5,000 P14 or SMARTA T cells. In some experiments, mice were seeded with both populations simultaneously. 1 d later, mice were infected i.p. with 10^5 PFU of LCMV Arm and considered memory donors at >45 d after infection.

Q-PCR. Brain tissue or FACS-sorted microglia were collected in TRIzol (Invitrogen), and total RNA was extracted using PureLink RNA Mini or Micro kits (Life Technologies) per the manufacturer's instructions. Purified RNA was then treated with amplification-grade DNase I (Invitrogen) to remove contaminating DNA and reverse transcribed into cDNA by using an iScript cDNA Synthesis kit (Life Technologies). Real-time PCR was performed using SYBR Green (Applied Biosystems) and cDNA template or water (nontemplate negative control) at an optimized annealing temperature (Table S1) with a CFX96 Real-Time PCR machine (Bio-Rad Laboratories). All reactions were conducted in triplicate, and PCR products were subjected to melt analysis to confirm purity after DNA amplification. For each gene, expression values were normalized to a β-actin control. The resulting relative gene expression was then expressed as a fold-change from the naive control samples. Primers were designed and obtained from Integrated DNA Technologies (IDT), and sequences are provided in Table S1.

Mononuclear cell isolations. Anesthetized mice received an intracardiac perfusion with PBS or saline to remove all contaminating blood lymphocytes. Afterward, brain, liver, and spleen tissues were harvested and then cut into small pieces, enzymatically digested with 2 ml collagenase D (1 mg/ml; Roche) + DNase (50 µg/ml; Roche) in RPMI medium for 30 min at 37°C, and finally passed through a 100-µm pore cell strainer. Brain-infiltrating mononuclear cells were isolated by centrifugation on a 90/60/40% discontinuous Percoll (GE Healthcare) gradient in HBSS as described previously (Lauterbach et al., 2006). Single cell suspensions from spleen were prepared by mechanical disruption through a 100-µm strainer followed by red blood cell lysis with ammonium chloride buffer (0.017 M Tris-HCl and 0.14 M NH_4Cl, pH 7.2). To isolate liver-infiltrating leukocytes, homogenates were resuspended in 35% Percoll and centrifuged.

Flow cytometry. For surface staining, cells were incubated for 20 min on ice with cocktails of mAbs in PBS containing 2% FBS. Before staining, all cell preparations were incubated with 3.3 µg/ml rat anti–mouse CD16/32 (Fc receptor block; BD) and 1:50 whole mouse IgG (Jackson ImmunoResearch Laboratories, Inc.) for 10 min on ice to reduce unspecific antibody binding. Dead cells were excluded from the analysis by using the LIVE/DEAD fixable Blue Cell Staining kit (Invitrogen). The following antibodies were obtained from BioLegend (BL), BD, or eBioscience (eB): CD4 Brilliant Violet 605 (RM4-5; BL), CD8α Alexa Fluor 700 (53-6.7; BL) or Pacific Blue (5H-10; Invitrogen), CD11b Brilliant Violet 605 (M1/70; BL) or PECy7 (M1/70; eB), CD11c APCCy7 (N418; BL), CD39 PECy7 (24DMS1; eB), CD45.2 FITC or Alexa Fluor 700 (104; BD), H-$2K^bD^b$ Alexa Fluor 647 (28-8-6; BL), I-A/I-E PerCPCy5.5 (M5/114.15.2; BL), Ly6C APCCy7 (HK1.4; BL), Ly6G PE or Pacific Blue (1A8; BL), Thy1.1 PECy7 (HIS51; eB) or PE (OX-7; BL), Thy1.2 APC or Alexa Flour 700 (30-H12; BL), and matching isotype controls. For detection of apoptotic cells, single cell suspensions were stained with Annexin V Alexa Fluor 647 (BL) and propidium iodide (BD) per the manufacturer's instructions. For intracellular staining to detect granzyme B, CXCL9, CCL5, and LCMV, single cell suspensions were first stained with surface antibodies, then treated with Cytofix/Cytoperm (BD), and stained intracellularly with anti–human granzyme B PE (GB11; Invitrogen), CXCL9 eFluor660 (MIG-2F5.5; eBioscience), anti–mouse CCL5 (purified polyclonal goat IgG; R&D Systems), and anti–mouse LCMV (VL-4; Bio X Cell). Anti-LCMV mAb was directly conjugated to Alexa Fluor 647 using an antibody-labeling kit from Invitrogen. Anti-CCL5 was detected by staining cell suspensions with a secondary anti–goat DyLight 647 (Jackson ImmunoResearch Laboratories, Inc.). For labeling of proliferating microglia, mice were injected i.p. daily with BrdU (Sigma-Aldrich) in sterile 1× PBS for 8 d at a dose of 1 mg per animal. BrdU incorporation into cycling microglia was detected using the APC BrdU Flow kit (BD) per the manufacturer's instructions. Samples were acquired using an LSR II flow cytometer (BD), and data were analyzed using FlowJo software version 9.7.6 (Tree Star).

Isolation of microglia. Microglia were isolated from CX3CR1-$GFP^{+/-}$ carrier and day 12 CD11c-YFP^+ immunotherapy recipient mice using a FACSAria Digital Cell Sorter (BD). Brain-infiltrating mononuclear cells were extracted and stained as described in the Mononuclear cell isolation and Flow cytometry sections above. Microglia were sorted to >99% purity based on the following markers: 7-AAD^- $Thy1.2^-$ $CD45.2^{lo}$ $CD11b^+$ $Gr1^-$ $CD39^+$ CX3CR1-GFP^+ (carrier mice) or CD11c-YFP^+ cells (immunotherapy recipients).

Evans blue assay. To quantify vascular leakage, Evans blue (Sigma-Aldrich) was injected i.v. at a concentration of 20 mg/kg body weight diluted in PBS. After 4 h, brain and liver tissue were removed after perfusing mice with saline. Evans blue was extracted from tissues using *N,N*-dimethyl formamide (Sigma-Aldrich) as described previously (Kim et al., 2009). All samples were plated in triplicate on black 96-well flat-bottom plates (Corning), and fluorescence emission was quantified using a Varioskan Flash fluorometer (620-nm excitation; 695-nm emission; Thermo Fisher Scientific).

Immunohistochemistry. For immunohistochemical experiments, mice were perfused with saline or 4% paraformaldehyde (PFA) in PBS. The latter was used for all experiments involving tg fluorescent protein reporter mice. Tissue extracted from PFA-perfused mice was incubated overnight in 4% PFA in PBS and then for an additional 24 h in a sucrose solution (15% sucrose followed by 30% sucrose). Brain and liver tissue was then frozen on dry ice in Tissue-tek optimal cutting temperature medium (Thermo Fisher Scientific). 6-µm cryosections were fixed for 15 min with 2% PFA, washed three times with PBS, blocked with avidin-biotin blocking kit (Vector Laboratories) per the manufacturer's instructions, and stained with primary mAbs for 1 h at room temperature (RT) in PBS containing 2% FBS. The following were used as primary mAbs: mouse anti-NeuN (1:100; clone A60; EMD Millipore), rat anti-LCMV (1:1,000; clone VL-4; Bio X Cell), and rabbit anti–phospho-STAT1 Tyrosine 701 (1:100; clone 58D6; Cell Signaling Technology). Sections stained with anti-NeuN were preincubated for 1 h at RT with 35 µg/ml Fab anti–mouse H and L chain antibody (Jackson ImmunoResearch Laboratories, Inc.). After washing three times with PBS, tissue sections were stained with species-specific fluorescently conjugated secondary antibodies (1:400; Jackson ImmunoResearch Laboratories, Inc.) for 1 h at RT, washed, and costained with 10 ng/ml DAPI (Sigma-Aldrich) to label cell nuclei. Apoptotic cells were detected using the ApopTag Red In situ Apoptosis Detection kit (EMD Millipore) per the manufacturer's instructions. All slides were mounted with Vectashield (Vector Laboratories), and fluorescent images were acquired using an Axio Observer Z1 inverted epifluorescence microscope (Carl Zeiss) fitted with an automated xy stage and a 5× objective or an FV1200 confocal microscope (Olympus) equipped with an automated xyz stage, six laser lines (405, 458, 488, 515, 559, and 635 nm), and 4, 10, 20, and 40× objectives. The number of apoptotic cells per square millimeter of tissue was determined by first capturing tiled images of entire brain or liver sections using the "mosaic" function in the Zen microscope software (Carl Zeiss). Individual apoptotic cells were identified and enumerated using the "spots" tool in Imaris version 7.7 (Bitplane). The area of tissue sampled was calculated by manually drawing a region of interest in Zen around the tiled tissue sections identified by DAPI staining. The number of apoptotic cells was then divided by the total tissue area sampled. $pSTAT1^+$ neurons and $CD11c^+$ cells were enumerated in Imaris by calculating the frequency of $NeuN^+$ neurons or CD11c-YFP^+ cells with nuclear (identified by DAPI) pSTAT1 staining in

representative confocal images. A similar calculation was conducted using sections stained with an isotype control antibody to determine the level of background staining and tissue autofluorescence.

TPLSM. For imaging experiments, mice were anesthetized with chloral hydrate and perfused with cold artificial cerebral spinal fluid (aCSF; 119 mM NaCl, 26.2 mM $NaHCO_3$, 11 mM glucose, 2.5 mM KCl, 1 mM NaH_2PO_4, 1 mM Na-pyruvate, 0.4 mM sodium ascorbate, 1.3 mM $MgSO_4$, and 2.5 mM $CaCl_2$, pH 7.2). After gentle removal of brain tissue, 500-µm horizontal brain slices were cut with a Vibratome (Leica) into cold aCSF. Brain slices were then allowed to recover for 30 min at 35°C in oxygenated aCSF before placement into a temperature-controlled custom imaging chamber. To block MHC I–dependent interactions in brain slices, anti-H2 (clone M1/42.3.9.8; Bio X Cell) or isotype control antibodies (rat IgG2a) were added at a concentration of 500 µg/ml before imaging and every 30 min thereafter. While imaging, the tissue was held in place with a tissue harp (Warner Instruments) and constantly perfused with oxygenated aCSF warmed to a temperature of 35°C. 4D datasets were acquired using an SP5 two-photon microscope (Leica) equipped with two Mai Tai HP DeepSee lasers (SpectraPhysics), an 8,000-Hz resonant scanner, a 20×/1.0 NA objective, an NDD4 detector array, and a custom-environment chamber. Simultaneous excitation and detection of second harmonic (<458 nm), TFP (458–510 nm), YFP (510–562 nm), and OFP (>562 nm) was achieved using custom dichroic mirrors and by tuning one two-photon laser to 915 nm and the other to 990 nm. 3D stacks with a z step size of 2.5 µm and an xyz scan field of 300 × 300 × 150 µm were captured every 30 s. Stacks were captured at a depth of at least 50 µm below the cutting surface to avoid artifacts stemming from tissue injury. Imaging data were spectrally unmixed using the Application Suite AF software (Leica) and then processed with Imaris 7.7 software. Mean track velocities (µm/min), arrest coefficients, and meandering factors were calculated for all individual T cell tracks using Imaris 7.7 and T Cell Analyzer software (TCA 1.7.0; Strathclyde Institute of Pharmacy and Biomedical Sciences). The meandering factor was calculated by dividing the displacement of a cell by its total path length. Arrest coefficients were defined as proportion of time a cell spent arrested (<2 µm/min). The interaction duration between antiviral T cells and CD11c-YFP$^+$ microglia was defined as the amount of time the two populations spent in juxtaposition.

Microarray analysis. Total RNA was labeled on a sample-by-sample basis according to the manufacturer's guidelines for use with the Mouse Gene 2.0 ST Array (Affymetrix). Labeled cRNA were hybridized to these arrays in blinded interleaved fashion. The Scanner 3000 (Affymetrix) was used in conjunction with GeneChip Operation Software (Affymetrix) to generate one .CEL file per hybridized cRNA. These files have been deposited in the NCBI GEO database and are available for download (accession no. GSE66421). The Expression Console (Affymetrix) was next used to summarize the data contained across all .CEL files and generate 41,345 RMA normalized gene fragment expression values per file. Quality of the resulting values was challenged and assured via Tukey box plot, covariance-based PCA scatter plot, and correlation-based heat map using functions supported in "R" (http://www.cran.r-project.org). Lowess modeling of the data (CV∼mean expression) was performed to characterize noise for the system and discard gene fragments having noise-biased data (all RMA expression values <5.25). For gene fragments not discarded, differential expression between immunotherapy and control was tested for via Welch-modified *t* test. Gene fragments having both an uncorrected $P < 0.05$ by this test and an absolute difference of means ≥1.5× were subset as those having differential expression between immunotherapy and control (Fig. 6 A). Gene annotations for these subset fragments were obtained from Mouse Genome Informatics (MGI; The Jackson Laboratory) and IPA (Ingenuity). IPA was also used to identify the corresponding enriched functions and pathways for the genes (Fig. 6 B) and used to visualize network interactions for the genes (Fig. 6, C and D).

Statistical analysis. Statistical analyses for parametric data were performed using a Student's *t* test (two groups) or a one-way ANOVA (more than two groups) in Prism 6 (GraphPad Software) or Sigma Plot 11.0 software. Nonparametric data were analyzed using a Mann-Whitney *U* test. Groups were considered statistically different at a P-value of <0.05. All data are displayed as the mean ± SD.

Online supplemental material. Video 1 shows antiviral T cell interactions with CD11c$^+$ microglia after adoptive immunotherapy. Table S1 lists Q-PCR primer sequences used in this study. Table S2, included in a separate Excel file, shows differential gene expression in CD11c$^+$ microglia after immunotherapy. Online supplemental material is available at http://www.jem.org/cgi/content/full/jem.20142047/DC1.

This work was supported by the National Institutes of Health Intramural Research Program (to D.B. McGavern) and fellowship HE-6068/1-1 from the German Research Foundation (DFG; to J. Herz).

This work was supported by a grant from the National Institute of Arthritis and Musculoskeletal and Skin Diseases/National Institutes of Health (J.-H. Shim; 1 R01 AR068983-01). J.M. Penninger was supported by an Advanced European Research Council grant and an Innovator Award from the Era of Hope/Department of Defense.

The authors declare no competing financial interests.

Submitted: 29 October 2014
Accepted: 4 June 2015

REFERENCES

Ahmed, R., B.D. Jamieson, and D.D. Porter. 1987. Immune therapy of a persistent and disseminated viral infection. *J. Virol.* 61:3920–3929.

Anandasabapathy, N., G.D. Victora, M. Meredith, R. Feder, B. Dong, C. Kluger, K. Yao, M.L. Dustin, M.C. Nussenzweig, R.M. Steinman, and K. Liu. 2011. Flt3L controls the development of radiosensitive dendritic cells in the meninges and choroid plexus of the steady-state mouse brain. *J. Exp. Med.* 208:1695–1705. http://dx.doi.org/10.1084/jem.20102657

Barber, D.L., E.J. Wherry, D. Masopust, B. Zhu, J.P. Allison, A.H. Sharpe, G.J. Freeman, and R. Ahmed. 2006. Restoring function in exhausted CD8 T cells during chronic viral infection. *Nature*. 439:682–687. http://dx.doi.org/10.1038/nature04444

Berger, D.P., D. Homann, and M.B. Oldstone. 2000. Defining parameters for successful immunocytotherapy of persistent viral infection. *Virology*. 266:257–263. http://dx.doi.org/10.1006/viro.1999.0074

Bromley, S.K., D.A. Peterson, M.D. Gunn, and M.L. Dustin. 2000. Cutting edge: hierarchy of chemokine receptor and TCR signals regulating T cell migration and proliferation. *J. Immunol.* 165:15–19. http://dx.doi.org/10.4049/jimmunol.165.1.15

Brooks, D.G., M.J. Trifilo, K.H. Edelmann, L. Teyton, D.B. McGavern, and M.B. Oldstone. 2006. Interleukin-10 determines viral clearance or persistence in vivo. *Nat. Med.* 12:1301–1309. http://dx.doi.org/10.1038/nm1492

Bukowski, J.F., C.A. Biron, and R.M. Welsh. 1983. Elevated natural killer cell-mediated cytotoxicity, plasma interferon, and tumor cell rejection in mice persistently infected with lymphocytic choriomeningitis virus. *J. Immunol.* 131:991–996.

Bulloch, K., M.M. Miller, J. Gal-Toth, T.A. Milner, A. Gottfried-Blackmore, E.M. Waters, U.W. Kaunzner, K. Liu, R. Lindquist, M.C. Nussenzweig, et al. 2008. CD11c/EYFP transgene illuminates a discrete network of dendritic cells within the embryonic, neonatal, adult, and injured mouse brain. *J. Comp. Neurol.* 508:687–710. http://dx.doi.org/10.1002/cne.21668

Butovsky, O., S. Siddiqui, G. Gabriely, A.J. Lanser, B. Dake, G. Murugaiyan, C.E. Doykan, P.M. Wu, R.R. Gali, L.K. Iyer, et al. 2012. Modulating inflammatory monocytes with a unique microRNA gene signature ameliorates murine ALS. *J. Clin. Invest.* 122:3063–3087. http://dx.doi.org/10.1172/JCI62636

D'Agostino, P.M., C. Kwak, H.A. Vecchiarelli, J.G. Toth, J.M. Miller, Z. Masheeb, B.S. McEwen, and K. Bulloch. 2012. Viral-induced encephalitis initiates distinct and functional CD103$^+$ CD11b$^+$ brain dendritic cell populations within the olfactory bulb. *Proc. Natl. Acad. Sci. USA*. 109:6175–6180. http://dx.doi.org/10.1073/pnas.1203941109

Dow, C., C. Oseroff, B. Peters, C. Nance-Sotelo, J. Sidney, M. Buchmeier, A. Sette, and B.R. Mothé. 2008. Lymphocytic choriomeningitis virus infection yields overlapping $CD4^+$ and $CD8^+$ T-cell responses. *J. Virol.* 82:11734–11741. http://dx.doi.org/10.1128/JVI.00435-08

Fazakerley, J.K., P. Southern, F. Bloom, and M.J. Buchmeier. 1991. High resolution in situ hybridization to determine the cellular distribution of lymphocytic choriomeningitis virus RNA in the tissues of persistently infected mice: relevance to arenavirus disease and mechanisms of viral persistence. *J. Gen. Virol.* 72:1611–1625. http://dx.doi.org/10.1099/0022-1317-72-7-1611

Fischer, H.G., U. Bonifas, and G. Reichmann. 2000. Phenotype and functions of brain dendritic cells emerging during chronic infection of mice with *Toxoplasma gondii*. *J. Immunol.* 164:4826–4834. http://dx.doi.org/10.4049/jimmunol.164.9.4826

Friedman, R.S., P. Beemiller, C.M. Sorensen, J. Jacobelli, and M.F. Krummel. 2010. Real-time analysis of T cell receptors in naive cells in vitro and in vivo reveals flexibility in synapse and signaling dynamics. *J. Exp. Med.* 207:2733–2749. http://dx.doi.org/10.1084/jem.20091201

Gossa, S., D. Nayak, B.H. Zinselmeyer, and D.B. McGavern. 2014. Development of an immunologically tolerated combination of fluorescent proteins for in vivo two-photon imaging. *Sci. Rep.* 4:6664. http://dx.doi.org/10.1038/srep06664

Gottfried-Blackmore, A., U.W. Kaunzner, J. Idoyaga, J.C. Felger, B.S. McEwen, and K. Bulloch. 2009. Acute in vivo exposure to interferon-γ enables resident brain dendritic cells to become effective antigen presenting cells. *Proc. Natl. Acad. Sci. USA.* 106:20918–20923. http://dx.doi.org/10.1073/pnas.0911509106

Guidotti, L.G., and F.V. Chisari. 2001. Noncytolytic control of viral infections by the innate and adaptive immune response. *Annu. Rev. Immunol.* 19:65–91. http://dx.doi.org/10.1146/annurev.immunol.19.1.65

Guidotti, L.G., P. Borrow, A. Brown, H. McClary, R. Koch, and F.V. Chisari. 1999a. Noncytopathic clearance of lymphocytic choriomeningitis virus from the hepatocyte. *J. Exp. Med.* 189:1555–1564.

Guidotti, L.G., R. Rochford, J. Chung, M. Shapiro, R. Purcell, and F.V. Chisari. 1999b.Viral clearance without destruction of infected cells during acute HBV infection. *Science.* 284:825–829. http://dx.doi.org/10.1126/science.284.5415.825

Haller, O., G. Kochs, and F. Weber. 2006. The interferon response circuit: induction and suppression by pathogenic viruses. *Virology.* 344:119–130. http://dx.doi.org/10.1016/j.virol.2005.09.024

Herz, J., B.H. Zinselmeyer, and D.B. McGavern. 2012. Two-photon imaging of microbial immunity in living tissues. *Microsc. Microanal.* 18:730–741. http://dx.doi.org/10.1017/S1431927612000281

Heslop, H.E., M.K. Brenner, and C.M. Rooney. 1994. Donor T cells to treat EBV-associated lymphoma. *N. Engl. J. Med.* 331:679–680. http://dx.doi.org/10.1056/NEJM199409083311017

Horwitz, M.S., C.F. Evans, D.B. McGavern, M. Rodriguez, and M.B. Oldstone. 1997. Primary demyelination in transgenic mice expressing interferon-γ. *Nat. Med.* 3:1037–1041. http://dx.doi.org/10.1038/nm0997-1037

Howe, C.L., R.G. Lafrance-Corey, R.S. Sundsbak, and S.J. Lafrance. 2012. Inflammatory monocytes damage the hippocampus during acute picornavirus infection of the brain. *J. Neuroinflammation.* 9:50. http://dx.doi.org/10.1186/1742-2094-9-50

Jamieson, B.D., L.D. Butler, and R. Ahmed. 1987. Effective clearance of a persistent viral infection requires cooperation between virus-specific $Lyt2^+$ T cells and nonspecific bone marrow-derived cells. *J. Virol.* 61:3930–3937.

John, B., B. Ricart, E.D. Tait Wojno, T.H. Harris, L.M. Randall, D.A. Christian, B. Gregg, D.M. De Almeida, W. Weninger, D.A. Hammer, and C.A. Hunter. 2011. Analysis of behavior and trafficking of dendritic cells within the brain during toxoplasmic encephalitis. *PLoS Pathog.* 7:e1002246. http://dx.doi.org/10.1371/journal.ppat.1002246

Joly, E., and M.B. Oldstone. 1992. Neuronal cells are deficient in loading peptides onto MHC class I molecules. *Neuron.* 8:1185–1190. http://dx.doi.org/10.1016/0896-6273(92)90138-4

Joly, E., L. Mucke, and M.B. Oldstone. 1991. Viral persistence in neurons explained by lack of major histocompatibility class I expression. *Science.* 253:1283–1285. http://dx.doi.org/10.1126/science.1891717

Kägi, D., B. Ledermann, K. Bürki, R.M. Zinkernagel, and H. Hengartner. 1996. Molecular mechanisms of lymphocyte-mediated cytotoxicity and their role in immunological protection and pathogenesis in vivo. *Annu. Rev. Immunol.* 14:207–232. http://dx.doi.org/10.1146/annurev.immunol.14.1.207

Kang, S.S., and D.B. McGavern. 2008. Lymphocytic choriomeningitis infection of the central nervous system. *Front. Biosci.* 13:4529–4543. http://dx.doi.org/10.2741/3021

Kang, S.S., and D.B. McGavern. 2010. Microbial induction of vascular pathology in the CNS. *J. Neuroimmune Pharmacol.* 5:370–386. http://dx.doi.org/10.1007/s11481-010-9208-9

Karman, J., C. Ling, M. Sandor, and Z. Fabry. 2004. Initiation of immune responses in brain is promoted by local dendritic cells. *J. Immunol.* 173:2353–2361. http://dx.doi.org/10.4049/jimmunol.173.4.2353

Kim, J.V., S.S. Kang, M.L. Dustin, and D.B. McGavern. 2009. Myelomonocytic cell recruitment causes fatal CNS vascular injury during acute viral meningitis. *Nature.* 457:191–195. http://dx.doi.org/10.1038/nature07591

Knickelbein, J.E., K.M. Khanna, M.B. Yee, C.J. Baty, P.R. Kinchington, and R.L. Hendricks. 2008. Noncytotoxic lytic granule-mediated $CD8^+$ T cell inhibition of HSV-1 reactivation from neuronal latency. *Science.* 322:268–271. http://dx.doi.org/10.1126/science.1164164

Koff, W.C., D.R. Burton, P.R. Johnson, B.D. Walker, C.R. King, G.J. Nabel, R. Ahmed, M.K. Bhan, and S.A. Plotkin. 2013. Accelerating next-generation vaccine development for global disease prevention. *Science.* 340:1232910. http://dx.doi.org/10.1126/science.1232910

Kreutzfeldt, M., A. Bergthaler, M. Fernandez, W. Brück, K. Steinbach, M. Vorm, R. Coras, I. Blümcke, W.V. Bonilla, A. Fleige, et al. 2013. Neuroprotective intervention by interferon-γ blockade prevents $CD8^+$ T cell–mediated dendrite and synapse loss. *J. Exp. Med.* 210:2087–2103. http://dx.doi.org/10.1084/jem.20122143

Kunz, S., J.M. Rojek, A.J. Roberts, D.B. McGavern, M.B. Oldstone, and J.C. de la Torre. 2006. Altered central nervous system gene expression caused by congenitally acquired persistent infection with lymphocytic choriomeningitis virus. *J. Virol.* 80:9082–9092. http://dx.doi.org/10.1128/JVI.00795-06

Lauterbach, H., E.I. Zuniga, P. Truong, M.B. Oldstone, and D.B. McGavern. 2006. Adoptive immunotherapy induces CNS dendritic cell recruitment and antigen presentation during clearance of a persistent viral infection. *J. Exp. Med.* 203:1963–1975. http://dx.doi.org/10.1084/jem.20060039

Lauterbach, H., P. Truong, and D.B. McGavern. 2007. Clearance of an immunosuppressive virus from the CNS coincides with immune reanimation and diversification. *Virol. J.* 4:53. http://dx.doi.org/10.1186/1743-422X-4-53

Leen, A.M., G.D. Myers, U. Sili, M.H. Huls, H. Weiss, K.S. Leung, G. Carrum, R.A. Krance, C.C. Chang, J.J. Molldrem, et al. 2006. Monoculture-derived T lymphocytes specific for multiple viruses expand and produce clinically relevant effects in immunocompromised individuals. *Nat. Med.* 12:1160–1166. http://dx.doi.org/10.1038/nm1475

Lindquist, R.L., G. Shakhar, D. Dudziak, H. Wardemann, T. Eisenreich, M.L. Dustin, and M.C. Nussenzweig. 2004. Visualizing dendritic cell networks in vivo. *Nat. Immunol.* 5:1243–1250. http://dx.doi.org/10.1038/ni1139

Masopust, D., K. Murali-Krishna, and R. Ahmed. 2007. Quantitating the magnitude of the lymphocytic choriomeningitis virus-specific CD8 T-cell response: it is even bigger than we thought. *J. Virol.* 81:2002–2011. http://dx.doi.org/10.1128/JVI.01459-06

McGavern, D.B., and S.S. Kang. 2011. Illuminating viral infections in the nervous system. *Nat. Rev. Immunol.* 11:318–329. http://dx.doi.org/10.1038/nri2971

McGavern, D.B., U. Christen, and M.B. Oldstone. 2002a. Molecular anatomy of antigen-specific $CD8^+$ T cell engagement and synapse formation in vivo. *Nat. Immunol.* 3:918–925. http://dx.doi.org/10.1038/ni843

McGavern, D.B., D. Homann, and M.B. Oldstone. 2002b. T cells in the central nervous system: the delicate balance between viral clearance and disease. *J. Infect. Dis.* 186:S145–S151. http://dx.doi.org/10.1086/344264

McMahon, E.J., S.L. Bailey, C.V. Castenada, H. Waldner, and S.D. Miller. 2005. Epitope spreading initiates in the CNS in two mouse models of

multiple sclerosis. *Nat. Med.* 11:335–339. http://dx.doi.org/10.1038/nm1202

Merkler, D., E. Horvath, W. Bruck, R.M. Zinkernagel, J.C. Del la Torre, and D.D. Pinschewer. 2006. "Viral déjà vu" elicits organ-specific immune disease independent of reactivity to self. *J. Clin. Invest.* 116:1254–1263. http://dx.doi.org/10.1172/JCI27372

Mims, C.A. 1966. Immunofluorescence study of the carrier state and mechanism of vertical transmission in lymphocytic choriomeningitis virus infection in mice. *J. Pathol. Bacteriol.* 91:395–402. http://dx.doi.org/10.1002/path.1700910214

Moseman, E.A., and D.B. McGavern. 2013. The great balancing act: regulation and fate of antiviral T-cell interactions. *Immunol. Rev.* 255:110–124. http://dx.doi.org/10.1111/imr.12093

Müller, U., U. Steinhoff, L.F. Reis, S. Hemmi, J. Pavlovic, R.M. Zinkernagel, and M. Aguet. 1994. Functional role of type I and type II interferons in antiviral defense. *Science.* 264:1918–1921. http://dx.doi.org/10.1126/science.8009221

Nath, A., and K.L. Tyler. 2013. Novel approaches and challenges to treatment of central nervous system viral infections. *Ann. Neurol.* 74:412–422. http://dx.doi.org/10.1002/ana.23988

Nayak, D., K.R. Johnson, S. Heydari, T.L. Roth, B.H. Zinselmeyer, and D.B. McGavern. 2013. Type I interferon programs innate myeloid dynamics and gene expression in the virally infected nervous system. *PLoS Pathog.* 9:e1003395. http://dx.doi.org/10.1371/journal.ppat.1003395

Nayak, D., T.L. Roth, and D.B. McGavern. 2014. Microglia development and function. *Annu. Rev. Immunol.* 32:367–402. http://dx.doi.org/10.1146/annurev-immunol-032713-120240

Oldstone, M.B., P. Blount, P.J. Southern, and P.W. Lampert. 1986. Cytoimmunotherapy for persistent virus infection reveals a unique clearance pattern from the central nervous system. *Nature.* 321:239–243. http://dx.doi.org/10.1038/321239a0

Ousman, S.S., and P. Kubes. 2012. Immune surveillance in the central nervous system. *Nat. Neurosci.* 15:1096–1101. http://dx.doi.org/10.1038/nn.3161

Oxenius, A., M.F. Bachmann, R.M. Zinkernagel, and H. Hengartner. 1998. Virus-specific MHC class II-restricted TCR-transgenic mice: effects on humoral and cellular immune responses after viral infection. *Eur. J. Immunol.* 28:390–400. http://dx.doi.org/10.1002/(SICI)1521-4141(199801)28:01<390::AID-IMMU390>3.0.CO;2-O

Papadopoulos, E.B., M. Ladanyi, D. Emanuel, S. Mackinnon, F. Boulad, M.H. Carabasi, H. Castro-Malaspina, B.H. Childs, A.P. Gillio, T.N. Small, et al. 1994. Infusions of donor leukocytes to treat Epstein-Barr virus-associated lymphoproliferative disorders after allogeneic bone marrow transplantation. *N. Engl. J. Med.* 330:1185–1191. http://dx.doi.org/10.1056/NEJM199404283301703

Papadopoulou, A., U. Gerdemann, U.L. Katari, I. Tzannou, H. Liu, C. Martinez, K. Leung, G. Carrum, A.P. Gee, J.F. Vera, et al. 2014. Activity of broad-spectrum T cells as treatment for AdV, EBV, CMV, BKV, and HHV6 infections after HSCT. *Sci. Transl. Med.* 6:242ra83. http://dx.doi.org/10.1126/scitranslmed.3008825

Phares, T.W., S.A. Stohlman, D.R. Hinton, and C.C. Bergmann. 2012. Enhanced CD8 T-cell anti-viral function and clinical disease in B7-H1-deficient mice requires CD4 T cells during encephalomyelitis. *J. Neuroinflammation.* 9:269. http://dx.doi.org/10.1186/1742-2094-9-269

Pircher, H., K. Bürki, R. Lang, H. Hengartner, and R.M. Zinkernagel. 1989. Tolerance induction in double specific T-cell receptor transgenic mice varies with antigen. *Nature.* 342:559–561. http://dx.doi.org/10.1038/342559a0

Planz, O., S. Ehl, E. Furrer, E. Horvath, M.A. Bründler, H. Hengartner, and R.M. Zinkernagel. 1997. A critical role for neutralizing-antibody-producing B cells, $CD4^+$ T cells, and interferons in persistent and acute infections of mice with lymphocytic choriomeningitis virus: implications for adoptive immunotherapy of virus carriers. *Proc. Natl. Acad. Sci. USA.* 94:6874–6879. http://dx.doi.org/10.1073/pnas.94.13.6874

Plotkin, S.A. 2009. Vaccines: the fourth century. *Clin. Vaccine Immunol.* 16:1709–1719. http://dx.doi.org/10.1128/CVI.00290-09

Riddell, S.R., K.S. Watanabe, J.M. Goodrich, C.R. Li, M.E. Agha, and P.D. Greenberg. 1992. Restoration of viral immunity in immunodeficient humans by the adoptive transfer of T cell clones. *Science.* 257:238–241. http://dx.doi.org/10.1126/science.1352912

Rodriguez, M., M.J. Buchmeier, M.B. Oldstone, and P.W. Lampert. 1983. Ultrastructural localization of viral antigens in the CNS of mice persistently infected with lymphocytic choriomeningitis virus (LCMV). *Am. J. Pathol.* 110:95–100.

Sandberg, K., P. Kemper, A. Stalder, J. Zhang, M.V. Hobbs, J.L. Whitton, and I.L. Campbell. 1994. Altered tissue distribution of viral replication and T cell spreading is pivotal in the protection against fatal lymphocytic choriomeningitis in mice after neutralization of IFN-α/β. *J. Immunol.* 153:220–231.

Sanderson, N.S., M. Puntel, K.M. Kroeger, N.S. Bondale, M. Swerdlow, N. Iranmanesh, H. Yagita, A. Ibrahim, M.G. Castro, and P.R. Lowenstein. 2012. Cytotoxic immunological synapses do not restrict the action of interferon-γ to antigenic target cells. *Proc. Natl. Acad. Sci. USA.* 109:7835–7840. http://dx.doi.org/10.1073/pnas.1116058109

Santambrogio, L., S.L. Belyanskaya, F.R. Fischer, B. Cipriani, C.F. Brosnan, P. Ricciardi-Castagnoli, L.J. Stern, J.L. Strominger, and R. Riese. 2001. Developmental plasticity of CNS microglia. *Proc. Natl. Acad. Sci. USA.* 98:6295–6300. http://dx.doi.org/10.1073/pnas.111152498

Scholler, J., T.L. Brady, G. Binder-Scholl, W.T. Hwang, G. Plesa, K.M. Hege, A.N. Vogel, M. Kalos, J.L. Riley, S.G. Deeks, et al. 2012. Decade-long safety and function of retroviral-modified chimeric antigen receptor T cells. *Sci. Transl. Med.* 4:132ra53. http://dx.doi.org/10.1126/scitranslmed.3003761

Sedgwick, J.D., S. Schwender, H. Imrich, R. Dörries, G.W. Butcher, and V. ter Meulen. 1991. Isolation and direct characterization of resident microglial cells from the normal and inflamed central nervous system. *Proc. Natl. Acad. Sci. USA.* 88:7438–7442. http://dx.doi.org/10.1073/pnas.88.16.7438

Suvas, S., A.K. Azkur, and B.T. Rouse. 2006. Qa-1^b and CD94-NKG2a interaction regulate cytolytic activity of herpes simplex virus-specific memory $CD8^+$ T cells in the latently infected trigeminal ganglia. *J. Immunol.* 176:1703–1711. http://dx.doi.org/10.4049/jimmunol.176.3.1703

Tishon, A., H. Lewicki, G. Rall, M. Von Herrath, and M.B. Oldstone. 1995. An essential role for type 1 interferon-γ in terminating persistent viral infection. *Virology.* 212:244–250. http://dx.doi.org/10.1006/viro.1995.1477

Tyler, K.L. 2009a. Emerging viral infections of the central nervous system: part 1. *Arch. Neurol.* 66:939–948. http://dx.doi.org/10.1001/archneurol.2009.153

Tyler, K.L. 2009b. Emerging viral infections of the central nervous system: part 2. *Arch. Neurol.* 66:1065–1074. http://dx.doi.org/10.1001/archneurol.2009.189

van den Pol, A.N. 2006. Viral infections in the developing and mature brain. *Trends Neurosci.* 29:398–406. http://dx.doi.org/10.1016/j.tins.2006.06.002

Volkert, M. 1962. Studies on immunological tolerance to LCM virus. A preliminary report on adoptive immunization of virus carrier mice. *Acta Pathol. Microbiol. Scand.* 56:305–310. http://dx.doi.org/10.1111/j.1699-0463.1962.tb04909.x

Volkert, M. 1963. Studies on immunological tolerance to Lcm virus. 2. Treatment of virus carrier mice by adoptive immunization. *Acta Pathol. Microbiol. Scand.* 57:465–487. http://dx.doi.org/10.1111/j.1699-0463.1963.tb05115.x

Zhang, M., S.M. Park, Y. Wang, R. Shah, N. Liu, A.E. Murmann, C.R. Wang, M.E. Peter, and P.G. Ashton-Rickardt. 2006. Serine protease inhibitor 6 protects cytotoxic T cells from self-inflicted injury by ensuring the integrity of cytotoxic granules. *Immunity.* 24:451–461. http://dx.doi.org/10.1016/j.immuni.2006.02.002

Zinselmeyer, B.H., S. Heydari, C. Sacristán, D. Nayak, M. Cammer, J. Herz, X. Cheng, S.J. Davis, M.L. Dustin, and D.B. McGavern. 2013. PD-1 promotes immune exhaustion by inducing antiviral T cell motility paralysis. *J. Exp. Med.* 210:757–774.